ZnO Nanocones and Nanoplatelets: Synthesis and Characterization

A Thesis
Presented to
The Academic Faculty

by

Yanling Chang

In Partial Fulfillment
of the Requirements for the Degree
Masters of Science in the
School of Materials Science and Engineering

Georgia Institute of Technology

December 2010

ZnO Nanocones and Nanoplatelets: Synthesis and Characterization

Approved by:

Dr. Robert L. Snyder, Advisor
School of Materials Science and Engineering
Georgia Institute of Technology

Dr. W. Brent Carter
School of Materials Science and Engineering
Georgia Institute of Technology

Dr. Zhong Lin Wang, Co-Advisor
School of Materials Science and Engineering
Georgia Institute of Technology

Date Approved: July 29, 2010

To my entire family and friends

ACKNOWLEDGEMENTS

I would like to start off by thanking my thesis advisors, Dr. Snyder and Dr. Wang, for their guidance and support throughout the project. They have provided me with an incredibly amount of knowledge, taught and trained me how to perform research systemically. I could not have completed this work without their guidance. I would also like to thank Dr. Hong, Dr. Ding and Dr. Hu, who gave me helpful discussion, advice, training and assistance. Dr. Ding helped me with TEM measurement and Dr. Hu assisted me in electrical and optical measurement. I especially would like to thank Dr. Jung-Il Hong for serving as a mentor during this period. Dr. Carter also has my thanks for serving on my committee.

Next, I would like to thank my fellow group members for their support. They have been very kind and helpful and we have had numerous valuable discussions. Their advice and support have undoubtedly improved the quality of this research and we had a wonderful time with each other.

Finally, I would like to give my deepest thanks to my family and my friend Qiao. They always supported and encouraged me without any reservation, even though they do not understand what exactly I am doing. I really appreciated the courage they gave me when I first arrived in US.

Table of Contents

LIST OF TABLES

Page

LIST OF FIGURES

Page

SUMMARY

Nanowire structure plays an important role in the development of nanotechnology. However, further study shows that the shape of nanowires may not be the ideal morphology for some applications such as solar cells and sensors. Thus, the purpose of this thesis is to find a low cost and high yield approach to the synthesis of other morphologies of nanostructures in order to further improve the performance of these nanodevices.

To this end, a chemical approach has been extended to the synthesis ZnO nanocones and platelets. With UV illumination, the synthesis of ZnO nanocones was achieved on GaN films on sapphire and gold films on silicon substrates. Both TEM and XRD results show that as-grown ZnO nanocones are single crystals. The formation of ZnO nanocones could be explained by the absorption process of photons. The UV light induced thermal gradient modifies the heat distribution as well as the reagent transport. The chemical reaction system is kinetically limited and results in ZnO nanocones. If the UV light is blocked, the ZnO nanowires result. In addition, the density of ZnO nanocones is higher than ZnO nanowires grown without UV illumination.

By this chemical approach, ZnO platelets could also be obtained on GaN films deposited by PLD, whose c-axis is parallel to the surface of the substrate. The diameters and the thickness of the platelets depend on the quality and thickness of GaN film. TEM results illustrate that the obtained ZnO platelets are

single crystals grown along the <0 1 $\bar{1}$ 0> direction within the {0 0 0 1} planes. Relative growth rates of various facets were altered by the presence of [1 0 0] textured GaN film. The suppression of the growth along c axis can also be achieved by citrate anions as a structure-directing agent to adsorb selectively on ZnO basal planes. Electrical measurement shows that the resistance of ZnO platelets is about 20-40 GΩ and it is higher than that of ZnO nanowires. Piezoelectric potential calculation results also indicate that the piezoelectric potential is higher than for ZnO nanowires with the same external applied stress.

These procedures and results demonstrate an easy and low cost way to fabricate ZnO nanocones and platelets, which may aid the utilization of nanostructures in solar cells, sensors and other applications to further improve their performance.

Chapter 1
Introduction

1.1 General Properties of ZnO Nanomaterials and Applications

1.1.1 Crystal Structure of ZnO

Zinc oxide, a wide band gap semiconductor, has attracted a lot of interest and it has been actively studied in nanoscience and nanotechnology for several decades. In nature, there are three polymorphic forms of ZnO [1]: wurtzite (B4), cubic zinc blende (B3), and cubic rocksalt (B1) (see Figure 1.1).

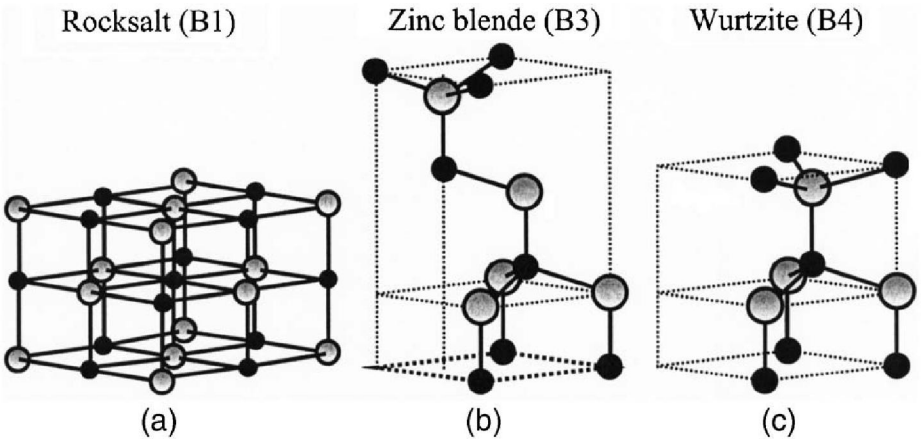

Figure 1.1: Stick and ball representation of ZnO crystal structures: (a) cubic rocksalt (B1), (b) cubic zinc blende (B3), and (c) hexagonal wurtzite (B4). The shaded gray and black spheres denote Zn and O atoms, respectively [1].

Wurtzite is the thermodynamically stable phase at ambient conditions. The zinc-blende ZnO structure can be stabilized only by growth on cubic substrates, and the cubic rocksalt structure of ZnO is only obtainable at high pressures of about 10GPa. The wurtzite structure of ZnO nanomaterials (see Figure 1.2) has a hexagonal unit cell with two lattice parameters of a = 0. 3296 nm and c = 0.52065 nm, in the ratio of c/a = $\sqrt{8/3}$ = 1.633 [1]. This structure is composed of two interpenetrating hexagonal-close-packed (hcp) sublattices, each of which consists of one type of atom displaced with respect to each other along the threefold c-axis by the amount of 0.375 in fractional coordinates. In other words, wurtzite ZnO can be described as a hexagonal close packing of oxygen with zinc atoms in tetrahedral sites and every atom of one kind is surrounded by four atoms of the other kind, or vice versa.

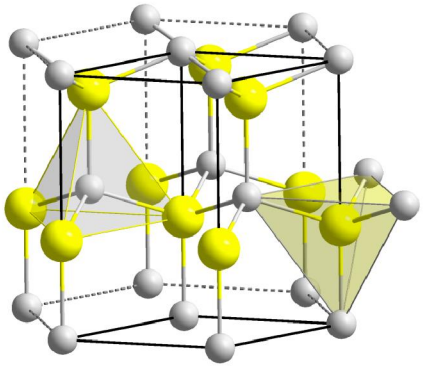

Figure 1.2: Schematic representation of a wurtzitic ZnO structure. The white and yellow spheres denote Zn and O atoms, respectively.

1.1.2 Piezoelectric Properties of ZnO

Wurtzite ZnO belongs to the point group 6mm and the space group of C_{6v}^4 or $P6_3mc$. This is a non-central symmetric structure so that the positive centers of zinc atoms do not correspond to the negative centers of oxygen atoms when it is pressed by external force. The separation of the central point of positive charges and that of negative charges leads to a temporary polarization, which is called piezoelectricity, a significant property of ZnO. Consequently, the concept of nanogenerators [2] was developed based on the coupling of piezoelectric and semiconductive properties of ZnO in the existence of a Schottky barrier between metal and the ZnO nanowires (See Figure 1.3 [2]).

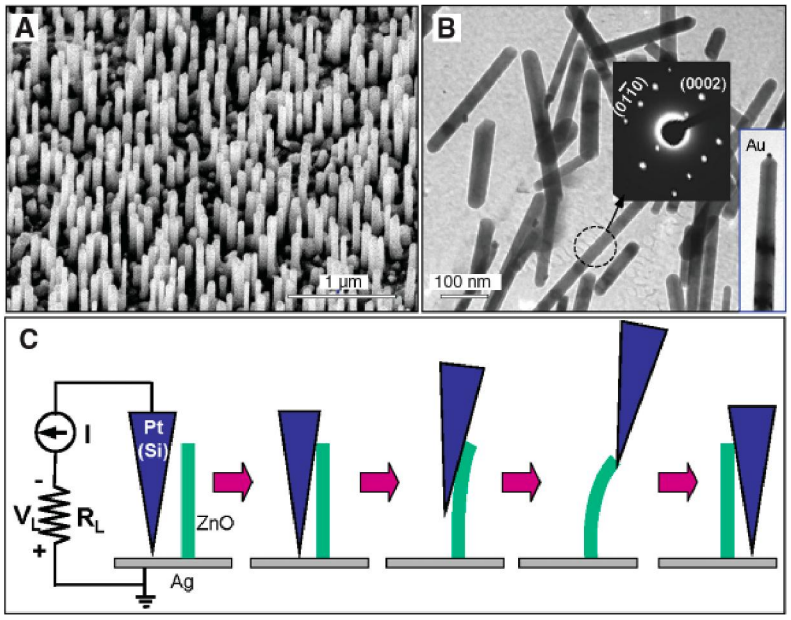

Figure 1.3: (a)The SEM images of ZnO nanowires; (b) TEM images of ZnO nanowires; (c) Experimental setup and procedures for generating electricity by deforming a piezoelectric ZnO nanowire with a conductive AFM tip [2].

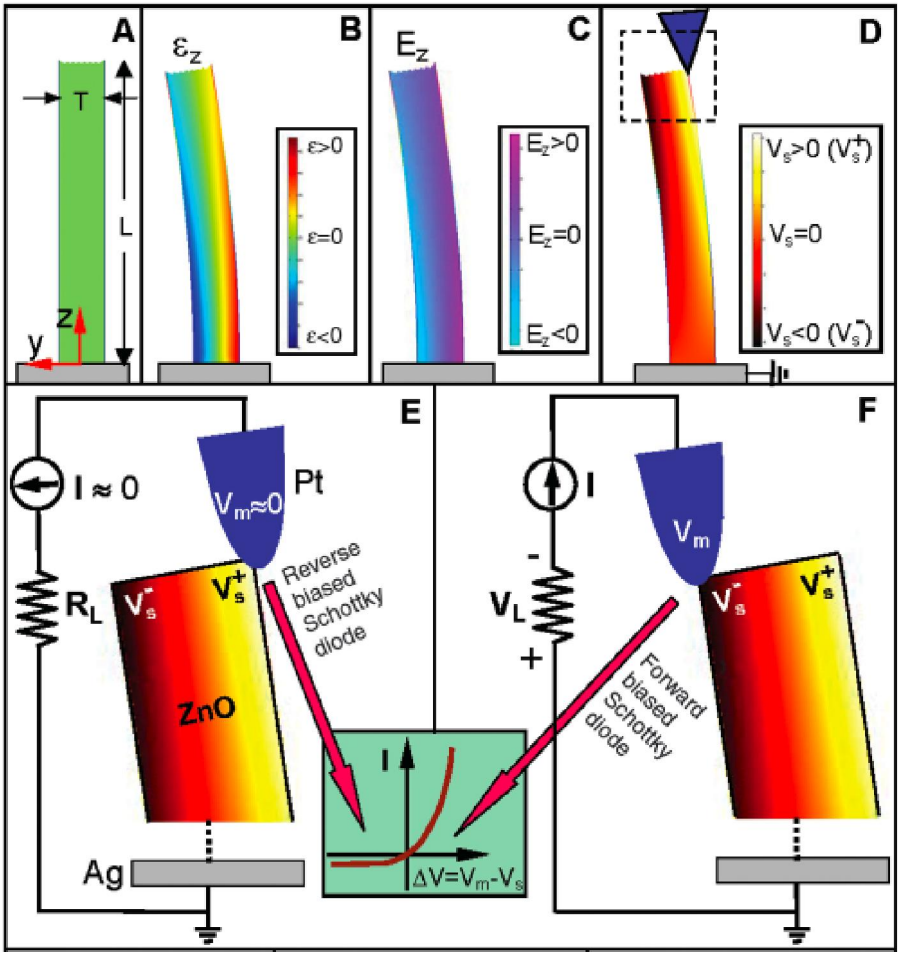

Figure 1.4: (a) Schematic definition of a nanowire and the coordination system; (b) The distribution of longitudinal strain (b)ε_Z (c) E_z (d)V_s in the nanowire after bending; (e) the process of current accumulation; (f) and the discharge model of nanogenerator [2].

When the Pt tip bends the vertical nanowire, there is a Schottky barrier between the nanowire and tip. The deflection of the nanowire by the tip creates a strain field, with the outer surface being stretched (positive strainε) and the inner surface compressed (negative strainε). Consequently, a positive piezoelectric potential V^+ is crated at its tensile surface and the reverse biased Schottky barrier blocks electrons. When the tip reaches the compressive side of the nanowire, the local potential drops to V^- (negative) and accumulated n-type

carriers in the nanowire that can quickly flow through contact to the tip, thus producing current flow. The presence of Schottky contacts at the tip-nanowire interface is mandatory for the operation of the nanogenerator, acting like a “gate” for separating and accumulating the charges as well as releasing the charge. The missing “gate” in the case of an Ohmic contact results in no charge accumulation and releasing, therefore no output signal is detected (see Figure 1.4 [2]).

The key element of the self-powered nanosystems for real-time and implantable biosensing, environmental monitoring, electromechanical systems and personal electronics is the power. The concept of the nanogenerator demonstrated an excellent route for harvesting energy from the environment by converting mechanical, chemical, or thermal energy into electricity. Up to now it has been shown that this kind of nanogenerator, with different configurations, could scavenge energy from several different sources such as mechanical vibration [3]-[7], biomechanical energy arising from small motions or the beating of a heart [8]-[11] and combined mechanical and biochemical energy [12]. In addition, in order to avoid the bottleneck problem in the application of nanogenerators, specifically the output power, novel designs of ZnO nanogenerators [13]- [14] and nanogenerators based on other materials such as GaN[15], CdS[16]-[17] and ZnS[18] have been developed and the output power has been substantially enhanced.

1.1.3 Electrical Properties of ZnO

ZnO is a direct and wide-band-gap material (3.37eV) with high exciton bonding energy (60meV) at room temperature and has many exciting electronic and optoelectronic applications such as lasers [19]-[21], light-emitting diodes [22]-[25], and solar cells [26]-[28]. There are several advantages associated with a large band gap such as the ability to sustain large electric fields, lower noise generation, higher breakdown voltages and high temperature and high-power operation. Normally people assess electron transport properties under low and high electric fields [1]. At sufficiently low electric field, the energy gained from the external electric field is so small compared to the thermal energy of the electrons that the energy distribution of the electrons is not affected. Consequently, the electron mobility remains independent of the applied electric field. On the contrary, at high electric field, the energy gained from the external electric field is high compared to the thermal energy of the electrons, so the electron distribution changes significantly from its equilibrium values. When the electron temperature is higher than the lattice temperature, these electrons become hot electrons. In addition, the ballistic or velocity overshoot phenomenon will show up when the dimensions of the device are decreased to submicron range where transient transport occurs. In this case, the loss to the lattice will be minimized or even vanish during a short and critical period of time and the electron drift velocity is higher than its steady-state value.

For semiconductor materials, the Hall effect is the effective way to measure the transport properties such as the carrier concentration, its type and carrier mobility as well as the quantitative information on impurities, imperfections, uniformity, scattering mechanisms, etc. The Hall coefficient R_H and resistivity ρ could be experimentally determined. Then the electrical parameters such as the free electron concentration n, Hall mobility μ_H and drift mobility μ could be obtained through $R_H = \frac{r_H}{ne}$, $\mu_H = \frac{R_H}{\rho}$ and $\mu_H = r_H\mu$ where r_H is the Hall scattering factor that is dependent on the particular scattering mechanism. There are five major scattering mechanisms: (1) Ionized impurity scattering; (2) Polar LO-phonon scattering; (3) Acoustic-phonon scattering; (4) Piezoelectric scattering; (5) dislocation and native defects scattering. The reported room-temperature electron mobility of ZnO is ~ 300 cm^2/Vs assuming the Hall scattering factor to be unity [29]-[31]. Due to the presence of intrinsic or extrinsic defects such as the Zn interstitial (Zn_i) and the O vacancy (V_o), normally undoped wurtzite ZnO becomes an n-type semiconductor. $O_o^x \leftrightarrow \frac{1}{2}O_2(g) + V_o^{\cdot\cdot} + 2e'$ and $Zn_o^x \leftrightarrow Zn_i^{\cdot\cdot} + 2e'$. The highest room-temperature electron mobility for a bulk ZnO single crystal grown by a vapor-phase transport method is about 205 cm^2/Vs with a carrier concentration of $6.0 \times 10^{16} cm^{-3}$. The values of electron mobility and corresponding carrier concentration in bulk and thin-film ZnO grown by various techniques can be found in Table I[32]-[36].

Extensive work has been done to investigate the electrical transport properties of ZnO nanowires [37]-[59]. For example, the electrical properties as a

function of temperature could be obtained by fabricating field effect transistors based on a single ZnO nanowire. The current-voltage characteristics of a single ZnO nanowire were also measured in a metal-semiconductor-metal structure. The observed I-V characteristics were almost symmetric, rectifying or linear [40] (See figure 1.5 [40]).

Table 1.1: A compilation of XRD results, electron mobilities and corresponding carrier concentration obtained in nominally undoped bulk and thin-film ZnO deposited on different substrates by various growth techniques [32]-[36].

Sample	FWHM of XRD rocking curves (arc sec)	Carrier concentration (cm^{-3})	Electron mobility ($cm^2\ V^{-1}\ s^{-1}$)
Monte Carlo calculation	···	···	300
Bulk ZnO grown by vapor-phase transport method	n/a	6.0×10^{16}	205
Bulk ZnO grown by pressurized melt method	49 (0002)	5.05×10^{17} (296 K) 3.64×10^{16} (77 K)	131 (296 K) 298 (77 K)
Bulk ZnO grown by hydrothermal method	18 (0002)	8×10^{13}	200
ZnO thin film on *c*-plane sapphire substrates grown by PLD	151 (0002)	2.0×10^{16}	155
ZnO thin films on *c*-plane sapphire grown by MBE	42 (0002)	1.2×10^{17}	130
ZnO thin films grown on *a*-plane sapphire by MBE	n/a	7.0×10^{16}	120
$Zn_{0.9}Mn_{0.1}O$/ZnO heterostructure grown on *c*-plane sapphire by PLD	n/a	$8.8\times10^{12}\ cm^{-2}$	130
ZnO thin film on *c*-plane sapphire with ZnO/MgO double-buffer layers grown by MBE	18 (0002) 1076 ($10\bar{1}1$)	1.2×10^{17}	145
ZnO thin film grown on MgZnO-buffered $ScAlMgO_4$ substrates by PLD	<12 (0002) <12 ($10\bar{1}1$)	1×10^{16}	440

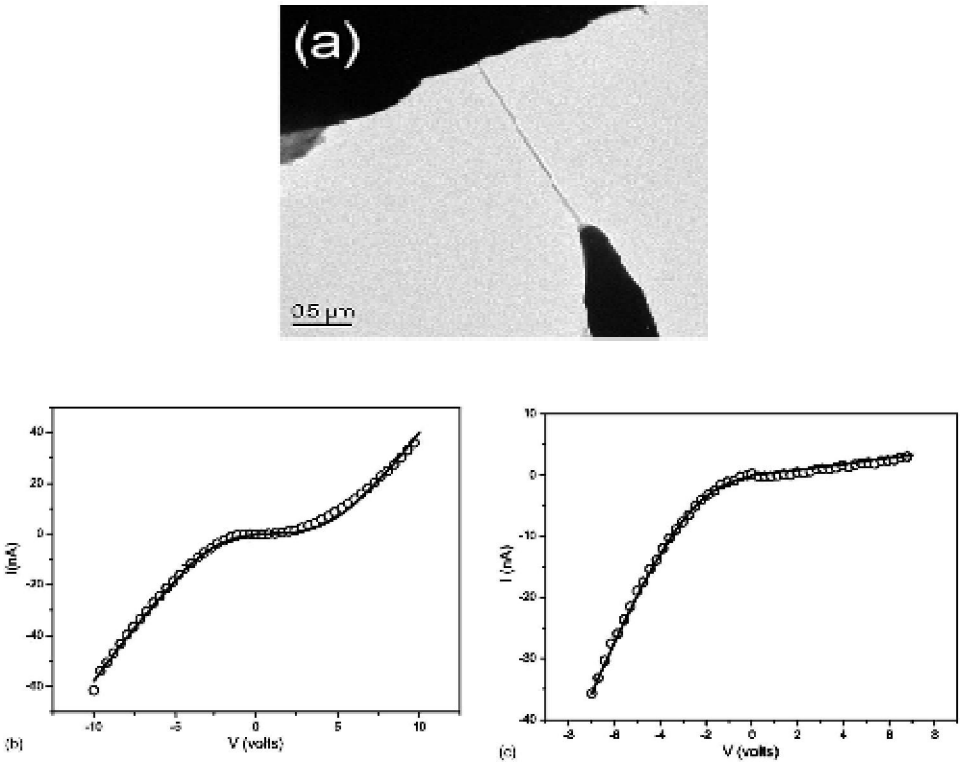

Figure 1.5: (a) TEM image of metal-ZnO nanowire-metal structure (b) symmetric I-V behavior (c) rectifying I-V behavior [40].

Table 1.2: Typical parameters for ZnO nanowires with length of 1.78 μm [40].

Parameter	ZnO
Bandgap (eV) 300 K	3.35
Mobility (bulk) (cm^2/V s)	200.0
Length (μm)	1.78
Diameter (nm)	40.8
E_0 (meV)	26.6
Electron concentration (/cm^3)	1.0E17
Resistivity (Ω cm)	7.06
Mobility (cm^2/V s)	8.85

It is worthy to notice that the reverse current in the nano-Schottky barrier structure is not negligible compared to the forward current. Traditionally in microelectronic system, the reverse current of an ideal Schottky junction should

saturate at a very low value and it is usually negligible. However, it is not the case in a nanosystem where the measured current is typically of the order of tens of nA that is comparable to that of the reverse or leakage current in a Schottky diode. Thus it cannot be explained by conventional thermionic emission theory. In fact, the tunneling current becomes the dominating mechanism under reverse bias, especially in low-dimensional systems [60]. Consequently, while the current through the forward biased Schottky barrier may be modeled by the classic thermionic emission current, people use thermionic field emission model of Padovani and Stratton to analyze the reverse-biased Schottky barrier [61]. The resistance of the nanowire can be determined by differentiating the I-V curve in a large bias regime. And it ranges from 10^{-3} Ω cm to 10^{5} Ω cm depending on the synthesis method [62]. In order to extract nanowire resistance, electron density and mobility, the part of I-V curves in the intermediate bias regime where the reverse-biased Schottky barrier dominates the total current I has to be used as follows [40]:

$$lnI = lnS + V\left(\frac{q}{kT} - \frac{1}{E_0}\right) + lnJ_s$$

where J is the current density through the Schottky barrier, S is the contact area associated with this barrier, E_0 is a parameter that depends on the carrier's density and J_s is a slowly varying function of applied bias. Electron concentration n can be obtained via E_0 and the electron mobility can be calculated from $\mu = \frac{1}{nq\rho}$ where ρ is the resistivity of the nanowire. The typical parameters for ZnO nanowires can be found in table 2 [40].

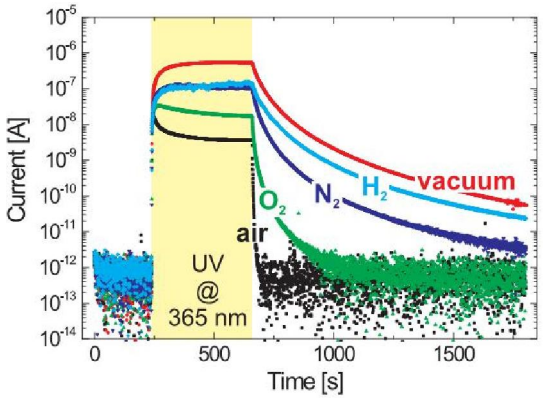

Figure 1.6: Influence of UV illumination on electrical resistance of ZnO measured in different atmospheres [64].

As we mentioned above, the variation of the resistivity is especially pronounced and there are numerous factors influencing the resistance measurements of the nanowires. Since a lot of electrical measurements were performed by two-probe measurement, the measured resistances must contain contributions from the resistances of the nanowires as well as from the contact resistances (Rc). Goldberger [48] has demonstrated that the contact resistance was about 2-10times the resistance of the nanowire. Although the ZnO nanowires are of single-crystalline quality, sometimes we could observe a considerably rough surface or crystalline imperfections in the outermost layer. This surface roughness may also influence the electrical properties of the nanowires. In addition, Schlenker [64] also pointed out that ambient conditions also significantly affect the electrical characteristics of ZnO. Nanowires possess a large surface-to-volume ratio so they are quite sensitive to variations in illumination, atmospheric composition and humidity. And he demonstrated the

changes of resistivity according to different atmospheric composition under UV illumination (see figure 1.6 [64]).

As a consequence of the sensitivity of ZnO nanowires to the presence of different gases during the measurement, ZnO nanowires were recognized as an excellent gas sensing materials [64]. Traditional, ZnO nanowire based gas sensors were constructed by two Ohmic contacts and Schottky contacts were usually avoided in order to enhance the contribution of the ZnO nanowires. Recently, however, non-symmetrical Schottky-contact devices of ZnO nanowires have been studied and found to have a giant enhancement in the sensitivity of several orders of magnitude over Ohmic-contact devices [65]. In this work, a single ZnO nanowire was bridged with one end in Ohmic contact and the other end in Schottky contact. Then the device was placed in Nitrogen atmosphere with 10 wt% Oxygen to investigate the sensitivity to the Oxygen. They recorded the response curve for the Ohmic contact device and reversely biased Schottky-contact device to the oxygen at different temperatures and analyzed the sensitivity and response time. (See figure 1.7 [65]). From these data, it is clearly seen that the performance of the Schottky-contact devices are much better than Ohmic contact devices for the gas sensor and the barrier height plays a key role for the greatly improved sensitivity. A maximum enhancement in sensitivity that was 4 orders of magnitude higher than that of the Ohmic-contact device could be observed with much faster response time. It is a new sensing mechanism that can be applied to other gas sensing systems in the future.

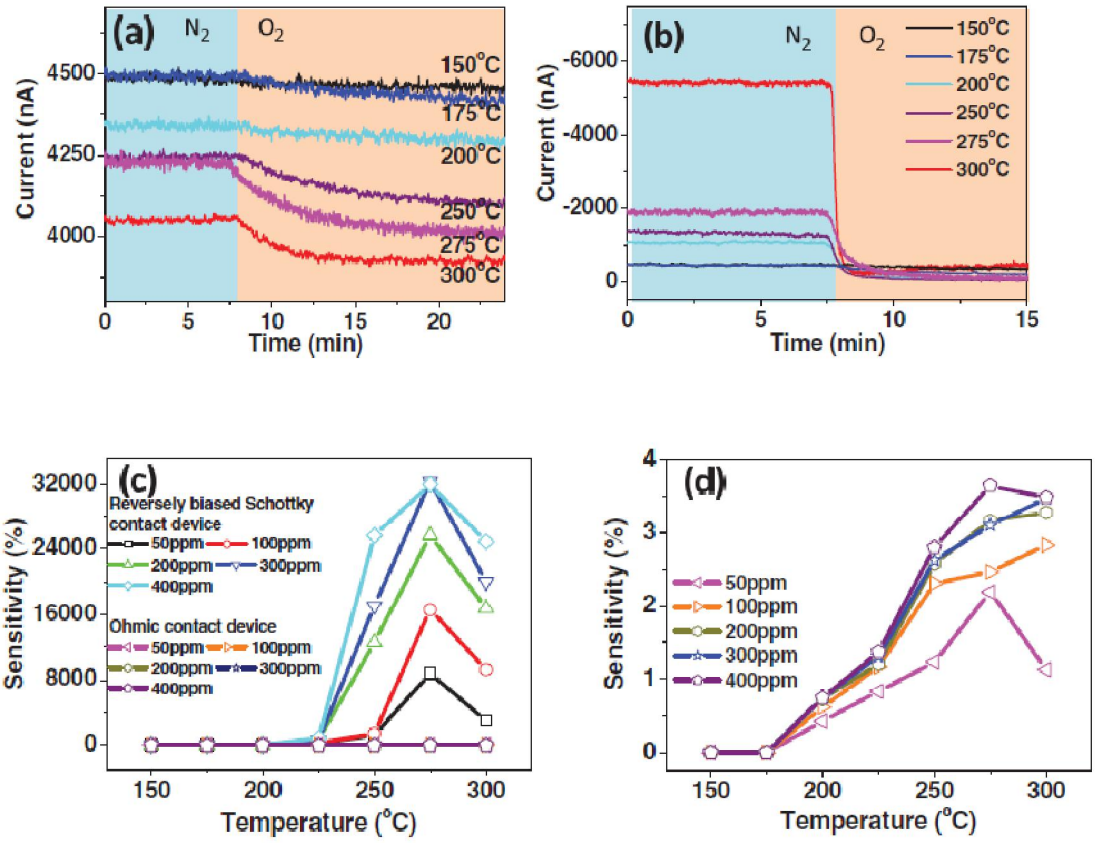

Figure 1.7: The response current of a ZnO NW (a) Ohmic-contact device, and (b) Schottky-contact device to the oxygen at different temperature. (c) Sensitivity comparison for the Ohmic-contact device and the Schottky-contact device with different concentrations of carbon monoxide at different temperature. (4) Magnification of the low sensitivity region of the Ohmic-contact device [65].

1.1.4 Optical Properties of ZnO

Both intrinsic and extrinsic effects have influence on the optical properties of a semiconductor. While intrinsic effects mean that the optical transition takes place between electrons in the conduction band and holes in the valance band, extrinsic effects are classified as free and bound excitons. If the impurities are introduced into the sample, discrete excited states and their ground states will

show up in their band structures, which influence both the optical-absorption and emission processes.

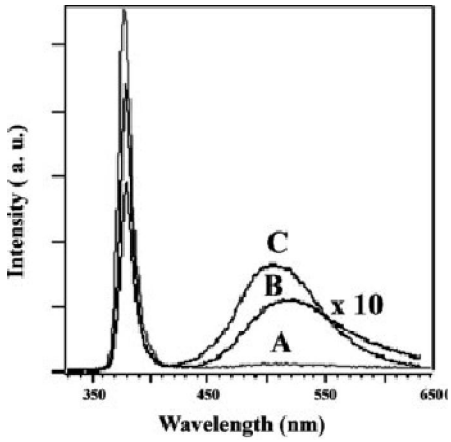

Figure 1.8: Room-temperature photoluminescence spectra of aligned ZnO nanowires array with different diameters (A: 100nm, B: 50nm, C: 25nm) [66].

A variety of technique has been exploited to investigate the optical transitions in ZnO nanowires. Room-temperature photoluminescence (PL) spectra of an aligned ZnO nanowires array shows that UV emission occurs at ~380nm and green emission at ~520nm due to the singly ionized oxygen vacancy is also noticeable (see Figure 1.8 [66]). The position of UV emission corresponds very well with the near band-edge emission of ZnO (the band gap of ZnO is 3.37 eV). And the green emission peak is commonly referred to as deep-level or trap-state emission [67], resulting from the radioactive recombination of a photo-generated hole with an electron occupying the oxygen vacancy. The smaller the diameter of the nanowires, the higher the green emission intensity.

The ratio of surface to volume is higher in thin nanowires than that of thick nanowires and a higher level of surface or sub-surface oxygen vacancy exist accordingly.

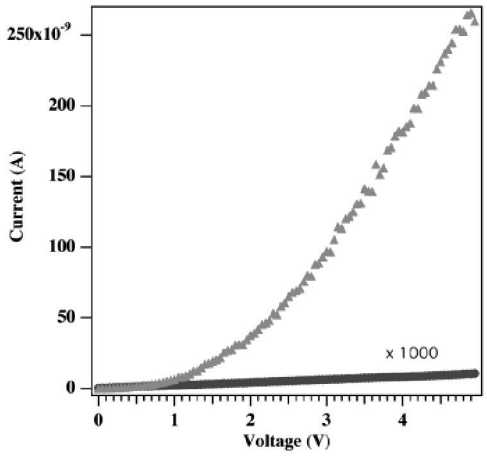

Figure 1.9: Comparison of currents in the dark and under UV illumination [68].

While ZnO nanowires are highly insulating in the dark, the resistivity of ZnO nanowires drops dramatically (approximately 4 to 6 orders of magnitude) when the nanowires are exposed to ultraviolet (UV)-light with wavelengths below 380 nm (See Figure 1.9 [68]). By now it is widely known that oxygen molecules tend to capture free electrons from the n-type ZnO and adsorb on the surface of nanowires as negatively charged ions. $O_2(g) + e^- \rightarrow O_2^-(ad)$. Consequently, a depletion layer is formed near the surface of the nanowires resulting in low conductivity in the dark. However, plenty of holes are produced upon exposure to UV-light and these holes can neutralize the adsorbed oxygen ions through

surface electron-hole recombination $h^+ + O_2^-(ad) \rightarrow O_2(g)$ and release these oxygen molecules. As a result, the depletion layer disappears the electrons generated from the photons also contribute to the current, thus the conductivity increases with the aid of UV illumination.

The optical characteristics of ZnO nanowires suggest that they are very good candidates for UV sensor or optoelectronic switches. The current significantly increases upon exposure to a UV source and returns to its back current when the source is turned off. (See Figure 1.10 [68]).

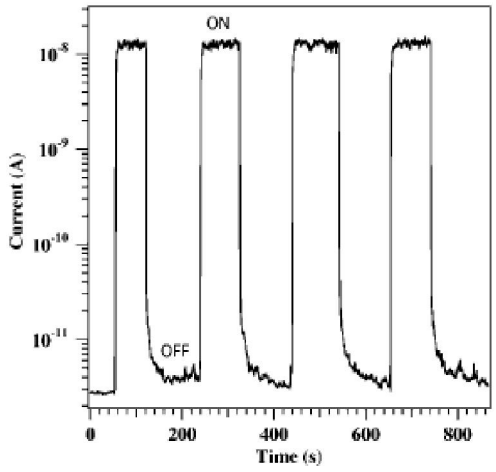

Figure 1.10: current responses to the switch of UV illumination [67].

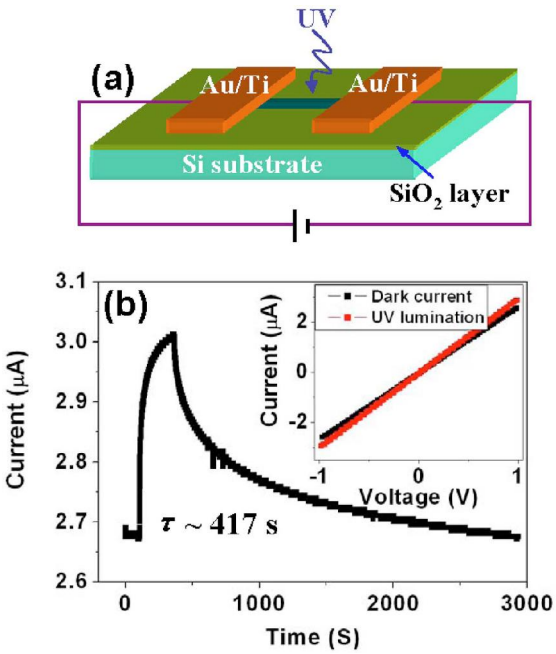

Figure 1.11: (a) Schematic of single ZnO NW UV detector with Ohmic contact. (b) current responses to UV illumination and its reset time, inset is the typical I-V curve with and without UV illumination [75].

This phenomena and mechanism has been widely studied [69]-[74] and substantial effort has been made to improve the sensitivity as well as the response and recovery (especially reset) time. A recent breakthrough is the work of Zhou [75]. He compared the UV sensitivity as well as the reset time for two different types of devices---Ohmic contact (See Figure 1.11 [75]) and Schottky contact (See Figure 1.12 [75]) and found that the Schottky type sensor can improve the sensitivity by four orders of magnitude and the reset time can be reduced to ~ 0.8s from ~417s. These results and mechanism indicate an effective way to further improve the performance of UV sensors.

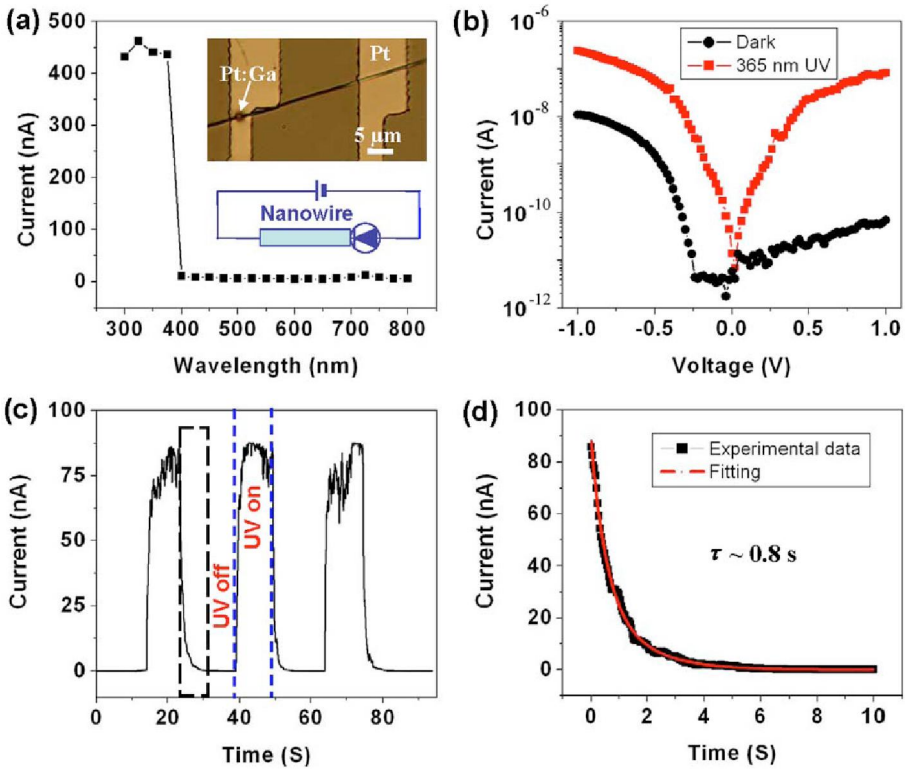

Figure 1.12: (a) Current response spectrum as a function of wavelength of incident light. Two insets are optical image and schematic structure of single ZnO NW UV detector with Schottky contact, respectively. (b) Typical I-V curve for Schottky type ZnO NW UV detector in the dark and under 365 nm UV illumination. (c) Current response to the switch of the UV illumination as a function of time. (d) Experimental and calculation results of photocurrent decay process [75].

1.1.5 Piezo-photonic-electronic Properties of ZnO Nanowires

While intensive work has been done to investigate the piezoelectric, electrical and optical properties of ZnO nanowires individually, little attention has been paid to the coupling among piezoelectricity, photonic excitation, and semiconductor transport. This coupling mechanism was first advanced by Dr. Z.L. Wang's group [76] and now it became the basis for the piezophototronics [77].

Piezophototronics is a novel concept such that it provides us a new approach to tune and control the electro-optical processes by a strain-induced piezopotential. To illustrate this concept, a two-end bonded single ZnO micro/nanowire device was fabricated [76]. Due to the variation of the local contact, the devices can be classified in three groups: (1) devices with Schottky-Ohmic contacts, (2) devices with Ohmic-Ohmic contact, and (3) devices with Schottky-Schottky contacts. The Schottky barrier is very sensitive to light which has energy larger than the band gap of ZnO and its height can be lowered with UV illumination. Such response in a device with both Ohmic contacts cannot be observed (See Figure 1.13 [76]). This is the photoexcitation effect.

Previous studies show that a piezoelectric potential gradient is introduced due to the polarization of the ions in the crystal when a stress parallel to the c-axis of the ZnO micro/nanowires is applied [78]. This piezoelectric field modifies the Schottky barrier heights for the two ends in the opposite direction and results in a nonsymmetric I-V transport property in micro/nanowires. Consequently, the diode-like I-V curve can be tuned to a totally off status across the entire voltage range by increasing the strain step-by-step (See Figure 1.14 [76]). This is the piezoelectric effect.

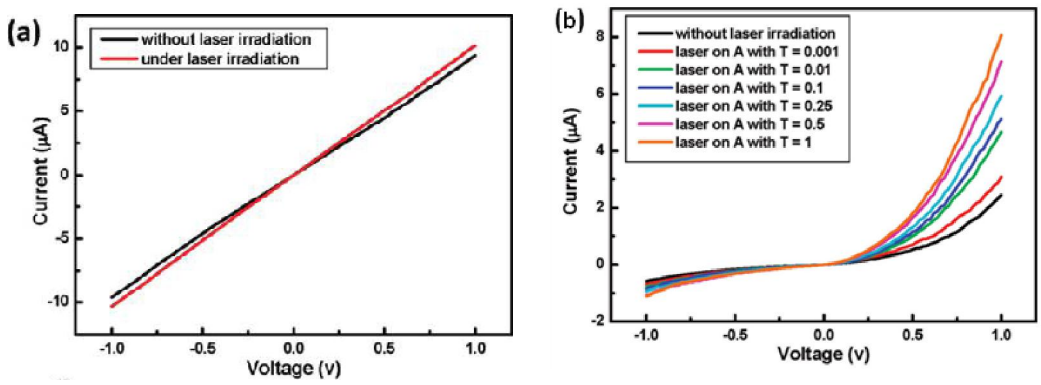

Figure 1.13: (a) I-V characteristic of devices with two Ohmic contacts, indicating that the response to the focused laser irradiation is negligible. (b) I-V characteristic of devices with Schottky contacts, indicating that the I-V characteristics can be tuned by controlling the intensity of the focused excitation laser. The transmission coefficient T ranges from 0.001 to 1, without strain [76].

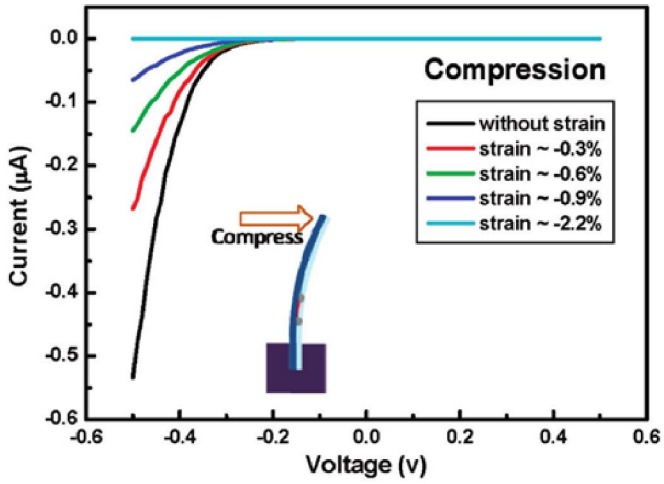

Figure 1.14: diode diode-like I-V curves can be tuned to a totally off status across the entire voltage range by increasing the strain step-by-step, without UV illumination [76].

As mentioned above, the two effects---piezoelectric effect and the photoexcitation---can tune the I-V characteristic of the devices for 3 different types in opposite directions. Thus, optical devices with the desired I-V characteristics could be obtained by suitably selecting the contributions of these

two competing mechanisms. For example, by choosing a relative light intensity of T=0.01 and a strain of -0.2 %, the I-V curve can go back to its original status, which is obtained in the dark without strain [76] (See Figure 1.15).

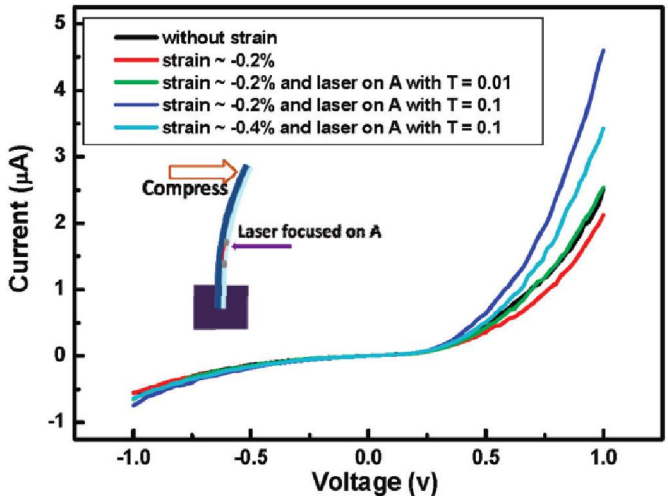

Figure 1.15: by choosing a relative light intensity of T=0.01 and a strain of -0.2 %, the I-V curve can go back to its original status, which is obtained in the dark without strain [76].

Piezophototronics results from the coupling among piezoelectricity, photonic excitation, and semiconductor transport and it has demonstrated its potential in tuning and controlling the electro-optical process by a strain-induced piezoelectric potential. The potential application includes light-emitting diodes, photocells, and solar cells [77], [79].

1.2 Motivation and Objectives

Besides carbon nanotubes and silicon nanowires, ZnO is one of the most interesting materials being actively studied in nanotechnology. Owing to its excellent mechanical, electrical, optical, piezoelectric properties, it has wide range of applications in energy harvesting, optoelectronics, sensors, actuators, biomedical sciences and so on.

Structurally, there are three types of fast growth directions in ZnO: $< 2\,\bar{1}\,\bar{1}\,0 >$, $< 0\,\bar{1}\,\bar{1}\,0 >$ and $< 0\,0\,0\,1 >$. A variety of novel structures of ZnO can be achieved by tuning the growth rates along these directions [80], including wire, ribbons, belts, springs, rings, diskettes and cages etc. (See figure 1.16).The capability of controlling the shape of nanostructures is very useful for building nanoscale devices.

Generally speaking, there are two approaches that can be utilized to create nanostructures with desired shapes: top down and bottom up. Top down approach is based on the rapid development of microelectronics and it refers to slicing or successive cutting of a bulk material to get nano sized particle. The yield of this approach is pretty high; however, problems like internal stress, surface defects, and contaminations are normally inevitable. The bottom up approach refers to the buildup of a material from the bottom such as atom by atom, molecule by molecule or cluster by cluster. This approach promises a

better chance to obtain nanostructures with less defects and a more homogeneous chemical composition.

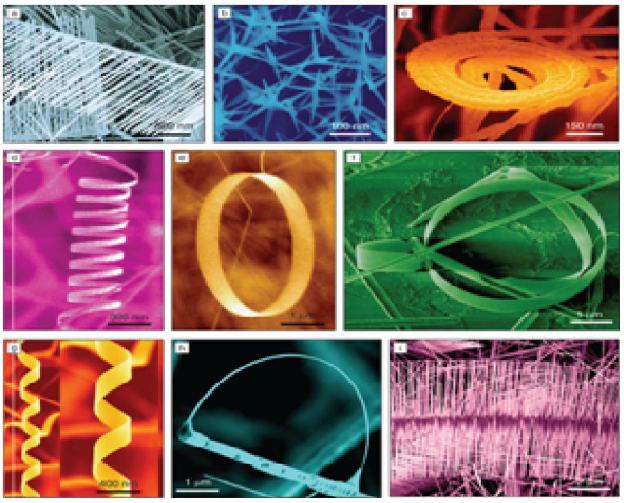

Figure 1.16: A collection of ZnO nanostructures: (a) Nanocombs or nanosaws, [81] (b) nano-tetrapoles, [82] (c) nanospirals, [83] (d) nanosprings, [84] (e) nanorings, [85] (f) a combination of nanoring and nanobow, [86] (g) nanohelices, [87] (h) nanobows, [88] and (i) double-sided nanosaws [89].

ZnO nanostructures can be synthesized by various methods such as laser vaporization, electrodeposition, and chemical or physical vapor deposition [90]-[93]. Vapor phase transport is an effective way to fabricate aligned ZnO nanowires arrays with low concentration of defects; however, it is usually achievable only at high temperature on single crystal substrates. On the contrary, a low temperature wet chemical method exhibits tremendous advantages over high temperature vapor deposition such as low cost, low temperature (< 100° C), polymer comparability, high yield, less experimental parameters and so on.

Among these chemical methods, Xu's work [94] demonstrated a novel and effective chemical approach to achieve density-controlled vertically aligned ZnO

nanowire arrays recently. Furthermore, the location, orientation, density, diameter and length can be controlled (See Figure 1.17 [95]) by e-beam lithography (EBL), which is a crucial step for future nanowire based electronic devices.

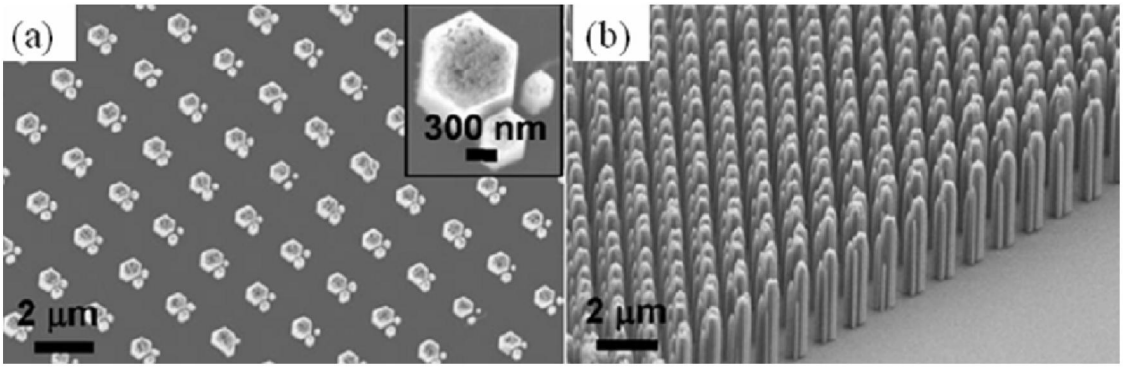

Figure 1.17: SEM images of (a) top view, and (b) tilted view of patterned ZnO nanowires arrays on GaN substrate without seedlayers [95].

The morphology of nanowires has a wide range of applications such as nanogenerators, single nanowire based strain sensors, biosensors, however, it may not be the ideal shape for some optical devices such as light-emitting diodes or solar cells. For example, in order to improve the efficiency of solar cells, conical shaped ZnO may be more suitable compared to nanowires since nanowire morphology leads to an abrupt change in refractive index that causes the strong reflection of light and low light absorption efficiency.

Contrary to one-dimensional nanostructures, 2D ZnO morphologies such as nanoplates also attract much attention and have potential applications in information storage, transducers, light emitters and sensors, especially when the devices have a requirement for polar surface area.

Although some work has been done to obtain these kinds of morphologies (see next chapter), the cost is always high and the procedures are complicated. Thus, the objective of this thesis is to promote a method that can modify the morphology of ZnO based on a low temperature chemical approach we mentioned above and to characterize these.

This thesis is organized as follows: In the next chapter, we will begin with the experiment procedure to form conical shaped ZnO nanowires by a chemical approach and then characterize this structure. In the third chapter, we will introduce a new method to synthesize the ZnO nanoplates and their property characterization. Finally, conclusions are drawn and recommendations for future work proposed.

Chapter 2

Synthesis of ZnO Nanocones and Characterization

2.1 Background

Carrier transport properties can be improved by advanced nanostructures, which are critical for enhancing the performance of semiconductor nanostructure applications such as radiation sensors, solar cells, and light-emitting diodes [96]-[99]. For dye-sensitized solar cells (DSCs), extensive work has been done recently based on nanowire electrodes [100]. A higher dye loading through an increase in surface area can be achieved using nanowires arrays. In addition, a nanowire electrode is expected to improve the quantum efficiency of DSCs in the red region of the spectrum because of the ordered topology that can increase the rate of electron transport. Consequently, the efficiency of the nanowire based solar cells can be raised to a competitive level.

Some of the most representative research is by Law et al published [99] in 2006. They applied the core-shell concept to a nanowire photoelectrode in order to increase the electron lifetime τ_n as well as the diffusion length of electrons $L_n$within the nanocrystalline oxide according to $L_n = (D_n\tau_n)^{1/2}$, thus maximizing red light conversion and boosting DSC efficiency. To fabricate the dye-sensitized

solar cells, they first fabricated ZnO nanowire arrays. Then thin shells of amorphous Al_2O_3 or anatase TiO_2 is coated on top of ZnO nanowires by atomic layer deposition (See figure 2.1 [99]).

An efficiency of 2.25 % under full sunlight can be achieved by ZnO-TiO_2 core-shell cells of optimal shell thickness and nanowire surface area. However, to further improve the efficiency of the solar cell, simply increasing the length or diameter of the nanowire may not be the right path since the array of core-shell nanowires with length of 30 μm, a core diameter of 40 nm, a shell thickness of 5 nm and a pitch of 70 nm would result in the same surface area as that of a typical nanocrystalline film.

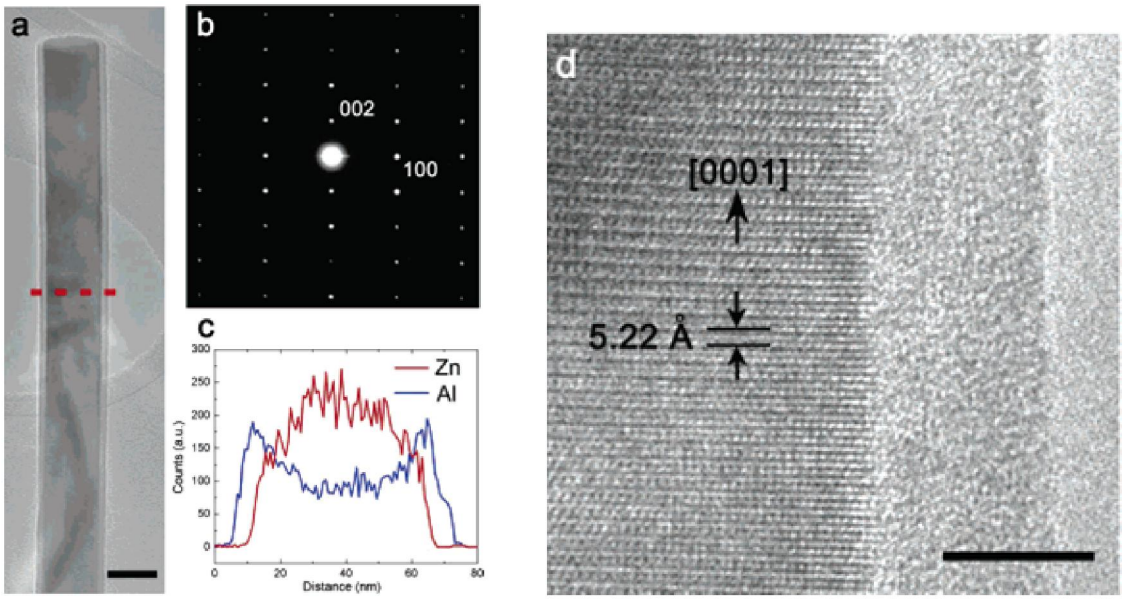

Figure 2.1: TEM images of ZnO-Al_2O_3 core-shell structure. (a) Low-magnification image of a wire coated with an amorphous layer. (b) Electron diffraction pattern of the wire, indicating only the ZnO pattern exists. (c) EDS spectrum for the wire. (d)High resolution image of the ZnO-Al_2O_3 interface [99].

Besides the surface area, the refractive index of the nanowires is another issue that needs to be settled. Take hydrogenated amorphous silicon for example, when light illuminates the surface of silicon, and a large portion of incident light is reflected back and thus cannot be captured to generate electricity. Although the application of antireflection coatings in industry can suppress reflection at a specific wavelength, we are aiming to achieve broadband reflection suppression [101]. Thus, several groups began to investigate the influence of the shape of nanostructures on the efficiency of the solar cell [99]-[102] to address such issues.

Zhu [101] investigated optical absorption in amorphous silicon nanowire and nanocone arrays. He calculated the effective refractive index profile for silicon thin films, nanowires arrays and nanocone arrays. The results showed that there is a huge and intermediate step in effective refractive index for thin film and nanowire arrays, respectively. The abrupt changes in refractive index will cause the reflection of light. However, for nanocone arrays, interesting things showed up. The diameter of these nanocones shrinks gradually from the root to the top, leading to a graded transition of the effective refractive index [101]. (See figure 2.2).Therefore, nanocones demonstrated the best antireflective properties and correspondingly the greatest absorption enhancement (See figure 2.3).

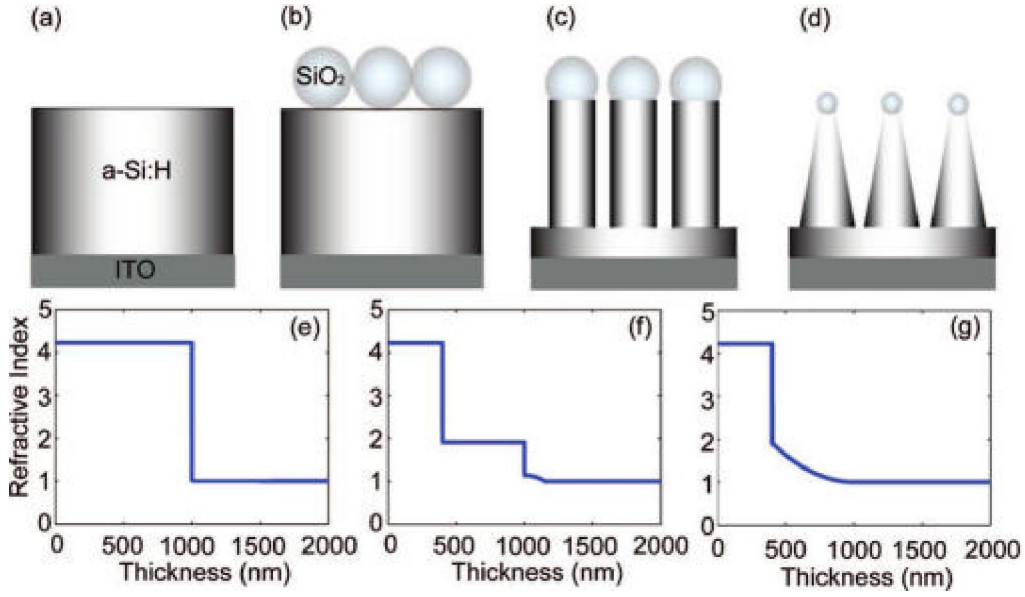

Figure 2.2: Schematic of (a,b) silicon thin film, (c) silicon nanowires array, (d) silicon nanocone arrays and their corresponding refractive index for (e) thin film, (f) nanowires, (g) nanocones[101].

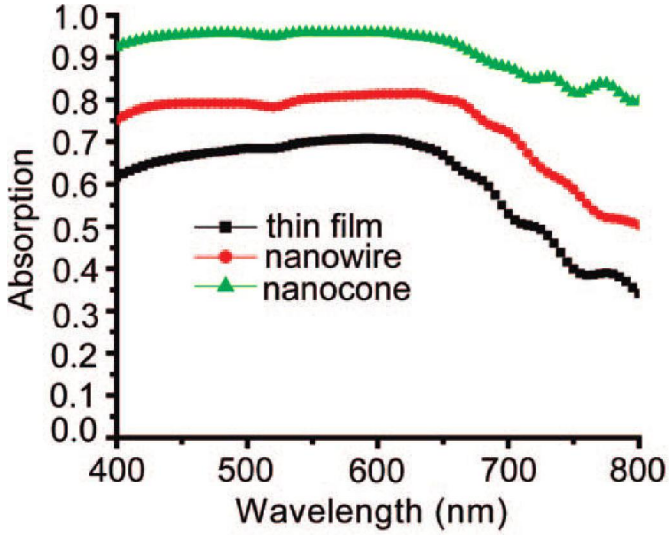

Figure 2.3: Comparison results of absorption as a function of wavelength for thin film, nanowire and nanocones [101].

Therefore, the nanocone structure is an ideal shape for harvesting light and is expected to be more efficient than the nanowire structure since the sides of the nanocones are tilted. This kind of structure can be achieved by a reactive ion etching process [101], pulsed-laser deposition [103], and thermal evaporation deposition [102], chemical etching [104] and so on. And in this section we promote a new method---a chemical approach with UV illumination---to synthesize ZnO nanocones.

2.2 Experiment Setup

Step 1: Substrate preparation

For this experiment, we used both Si (100) and GaN substrates. The procedure is quite similar to the approach we used to grow ZnO nanowires by a chemical method [94]. For the silicon substrate, a piece of silicon wafer was cleaned by a standard cleaning process. First, the wafer was consecutively ultrasonicated in acetone, ethanol, IPA (isopropyl alcohol), and de-ionized water for 10 mins each. Then the substrate was taken out and blown dry with nitrogen gas. It was placed on the hotplate at 100 ℃ for 10 mins to get rid of adsorbed moisture. Secondly, a 20 nm thick coating of Ti was deposited as an adhesion layer on top of silicon substrate by magnetron plasma sputtering. Then 50 nm thick Au was deposited on top of the Ti by DC sputter. The layer of Ti can buffer the large lattice mismatch between the silicon and the gold to improve the

interface bonding, otherwise the layer of gold will detach from the substrate (See figure 2.4). As for the GaN substrate, it can be used directly after cleaning.

Figure 2.4: Schematic of silicon substrate preparation

Step 2: Nutrient solution preparation

The nutrient solution is also the same as used for the synthesis of ZnO nanowires [94]. A 1:1 ratio of zinc nitrate and hexamethylenetetramine (HMTA) was dissolved in de-ionized water. These chemicals were purchased from Fluka (St. Louis, MO). The mechanism for the ZnO nanowire growth has been published [94]. Basically, zinc nitrate provides Zn^{2+} ions while water molecules provide O^{2-}ions to build up the ZnO nanostructure. There are five reactions involved as follow [94]:

$$(CH_2)_6N_4 + 6\,H_2O \leftrightarrow 4\,NH_3 + 6\,HCHO, \quad (1)$$

$$NH_3 + H_2O \leftrightarrow NH_3 \cdot H_2O, \quad (2)$$

$$NH_3 \cdot H_2O \leftrightarrow NH_4^+ + OH^-, \quad (3)$$

$$Zn^{2+} + 2\,OH^- \leftrightarrow Zn(OH)_2, \quad (4)$$

$$Zn(OH)_2 \rightarrow ZnO + H_2O. \qquad (5)$$

For ZnO nanowire growth, the density of ZnO nanowires can be controlled by the zinc precursor concentration. There is an optimal concentration at which the density of ZnO nanowires is maximized. Deviation from this concentration results in decreasing density of ZnO nanowires. At the same time, the growth temperature also affects the aspect ratio and morphology of the nanowires [94]. In our experiments, the reaction temperature of 85 ℃ was found to be the best one to grow ZnO nanowires.

Step 3: Beaker selection and UV light transmission test

The synthesis process is performed with the aid of UV illumination. Common laboratory beakers, however, block the UV transmission. Thus, it is necessary to choose a beaker through which most of the UV light can pass to reach the reaction surface between the gold film and reaction solution.

The UV lamp we used here is 100 watt long wave (365 nm) mercury spot lamp. (UVP P/N: 34-0054-01) The intensity at 2 inch and 10 inch distance is approximately 21,700 and 8,900 $\mu W / cm^2$, respectively (See Figure 2.5). The beakers used were bought from VWR. They have uniform thickness walls and are made of Type I, class A borosilicate glass.

Figure 2.5: 100 watt long wave mercury spot lamps

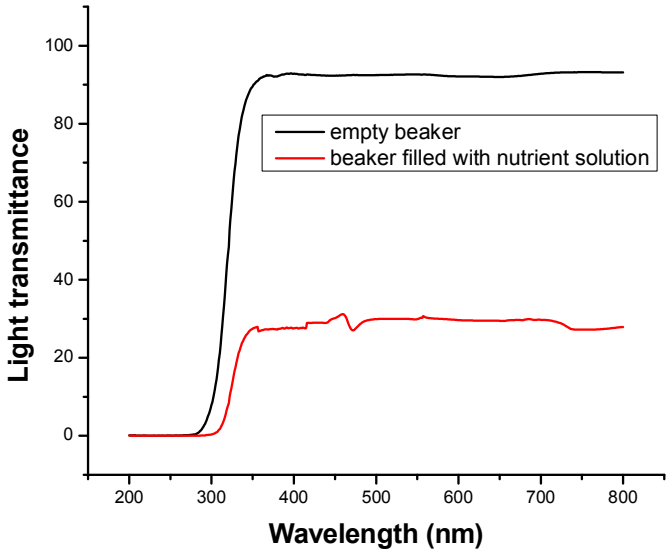

Figure 2.6: Light transmittance spectrum as a function of wavelength for empty beaker (black line) and beaker filled with nutrient solution (red line).

In order to investigate the light transparency of our setup, we scanned the light transmittance for the empty beaker as well as beaker filled with nutrient solution (See Figure 2.6) to see the percentage of light that can pass through the

beaker and the solution. The result in figure 2.6 shows that the light with wavelength higher than 350 nm can pass through the setup completely and it is only blocked with wavelengths shorter than 300 nm. Of course, the solution absorbs 70 percent of the light; there is still 30 percent left that can reach the reaction surface. This is sufficient since the power of the UV source is high.

Step 4: Reaction and Growth

The substrate was placed upside down and floated on the top of the solution surface due to surface tension. The UV lamp was placed under the beaker and the distance between the lamp and the surface of the substrate was about 10 inches. The substrate was just in the center of the UV light so the intensity was about 8,900 $\mu W / cm^2$. The whole setup was put in an oven and heated to 85 ℃. For comparison, nanowires were synthesized with the same conditions but without UV illumination.

The procedure is illustrated in figure 2.7.

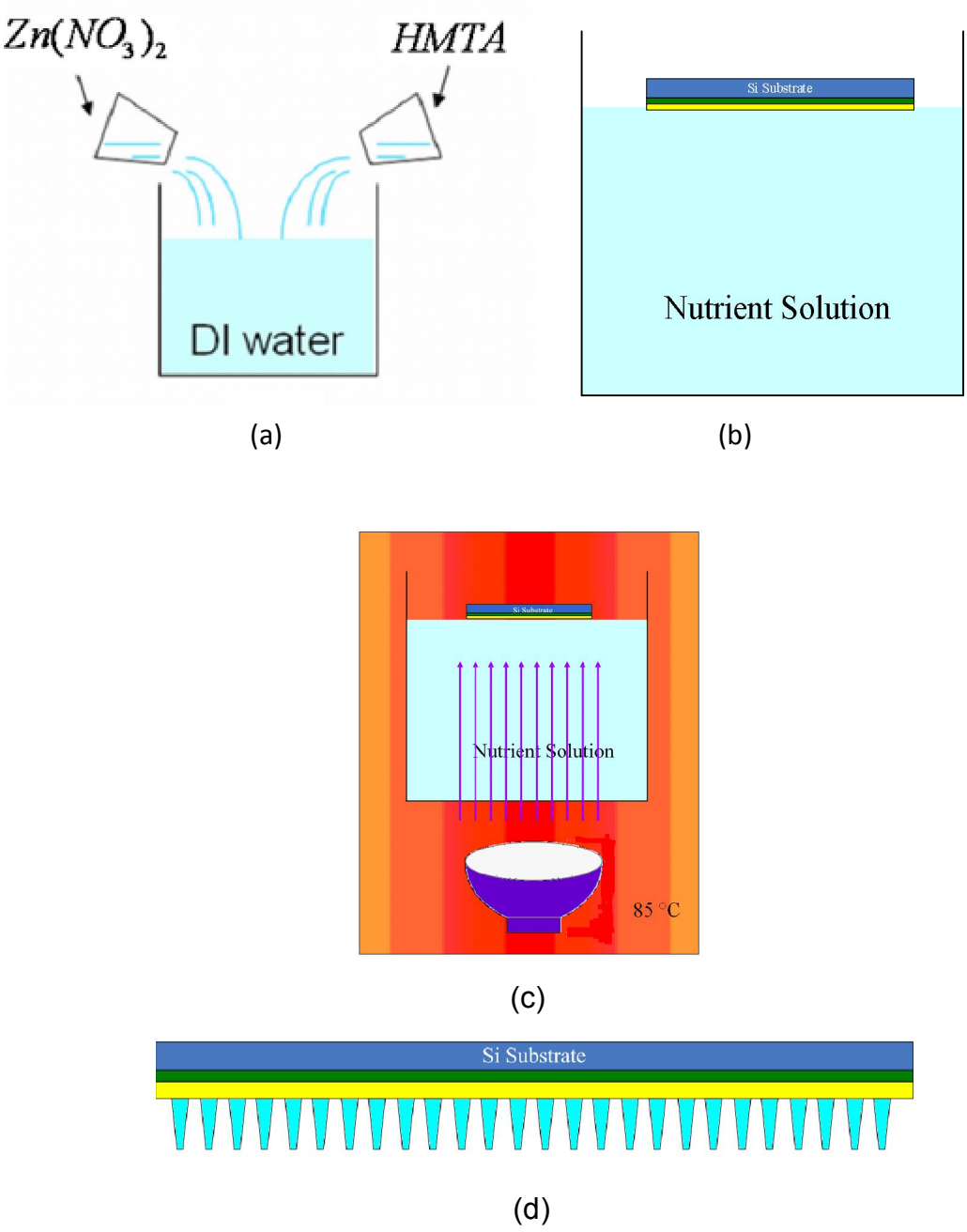

Figure 2.7: Schematic illustration of the process to synthesize ZnO nanocones.

2.3 Experimental Results

The samples were first observed using two scanning electron microscopes (SEM), a LEO 1530 and a LEO 1550. Both SEMS are equipped with thermally-assisted field emission guns, and imaging was conducted with the accelerating voltages generally being 5 kV. The samples did not require coating with gold or carbon to prevent excessive charging, even for the samples on insulating substrates such as undoped GaN substrates. The images in figure 2.8 clearly show that coating of ZnO nanocones was obtained on a large area. The ratio of the diameters of the tops to the bottoms was about 2 to 4.

The ZnO nanocone structures were further characterized by two different TEMs. We collected data (See Figure 2.9 (a)) at an accelerating voltage of 10kV with a JEOL 100CX II TEM, which is equipped with a tungsten filament. The maximum magnification of the JEOL 100CX II TEM is 320kX. High-resolution TEM (HRTEM) images can be obtained (See Figure 2.9 (b)) through a JEOL4000EX TEM at an accelerating voltage of 400kV. The maximum resolution of this TEM is 0.18 nm. These TEM images show that the single crystal structure of ZnO was not changed in the nanocone structure but the side surface of ZnO the nanocones was not as flat as for ZnO nanowires.

X-Ray scattering techniques were exploited to reveal crystallographic structure of the ZnO nanocones. The equipment we used is PANalytical X'Pert PRO Alpha-1 with 1.8 kW ceramic copper source X-ray tube. The detectors are

composed of Xe proportional counter and solid state X'cellerator. The acceleration voltage was 45 kV with a 40 mA current. For comparison, the XRD patterns were obtained for three samples: ZnO nanowires synthesized by the chemical approach, and ZnO nanocones synthesized by chemical approach with two levels intensity of UV illumination.

The results (see Figure 2.10) indicate that the preferred growth of the ZnO nanocones is along the c-axis, the same as ZnO nanowires. The two peak positions correspond to (1 0 0) and (0 0 2) planes. There is no significant difference among these diffraction patterns, although the intensity of (0 0 2) peak of ZnO nanocones obtained by UV illumination in full intensity is a little higher than others, indicating the better crystal quality. Also, the peak positions of some patterns may shift a little in some samples because of strain [105]. Strain in the crystal lattice influences the diffraction peaks. While nonuniform strain leads to peak broadening, uniform strain causes a peak position shift. Thus, there appears to be some uniform strain in the samples.

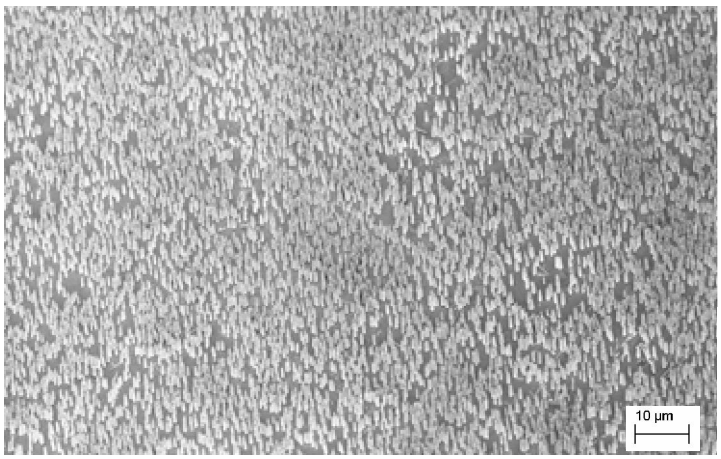

(a)

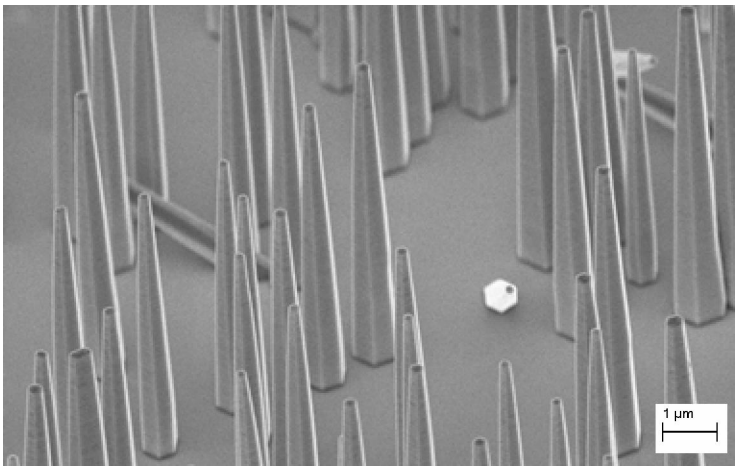

(b)

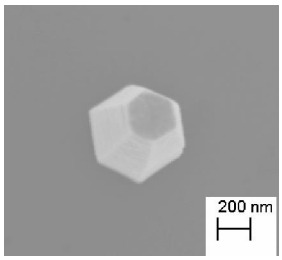

(c)

Figure 2.8: (a) SEM image (b) and (c) High magnification SEM image of ZnO nanocone synthesized by chemical approach with UV illumination.

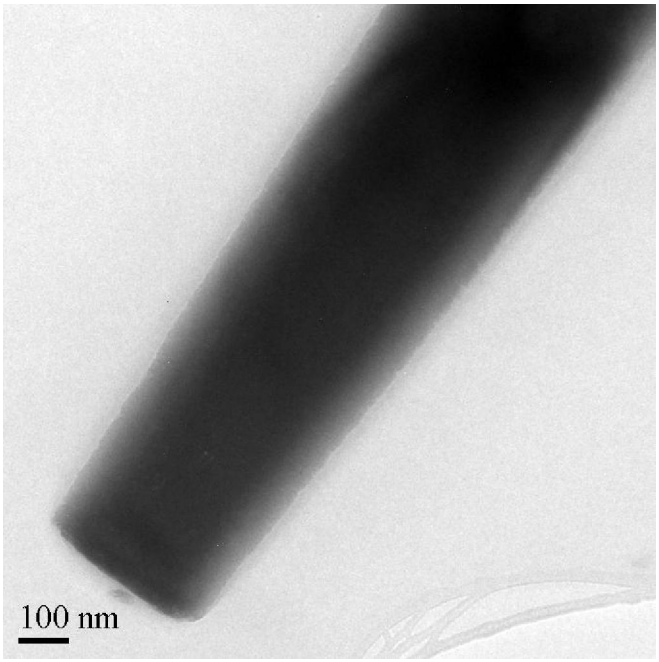

(a)

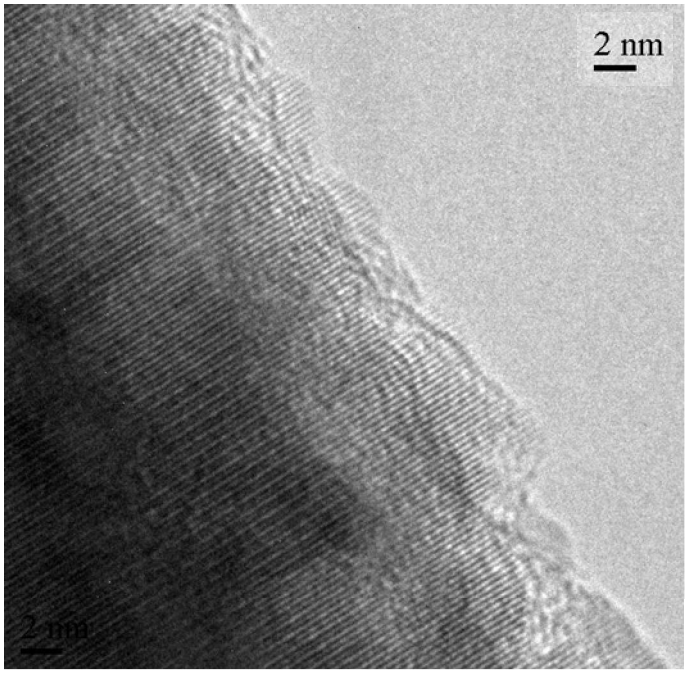

(b)

Figure 2.9: (a) Typical TEM image and (b) high-resolution TEM image of ZnO nanocone synthesized by chemical approach with UV illumination.

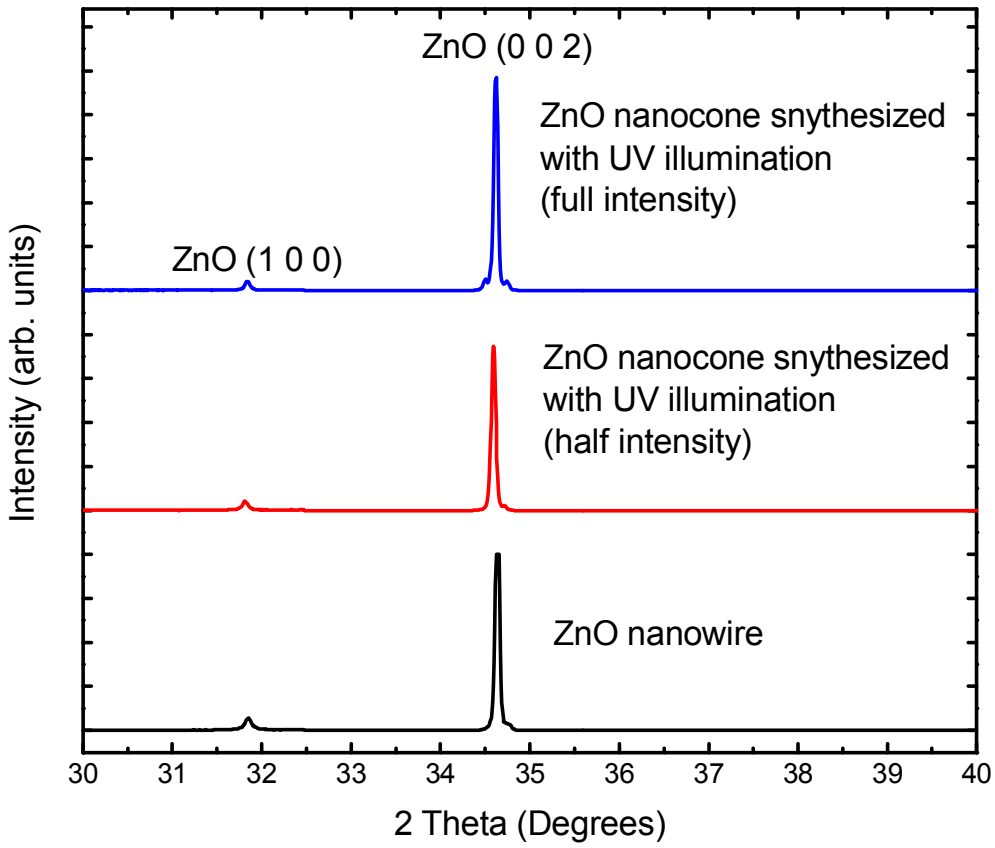

Figure 2.10: X-Ray diffraction patterns for ZnO nanowires and ZnO nanocone synthesized by chemical approach with UV illumination.

2.4 Discussion

In order to understand the growth mechanism for ZnO nanocones, SEM data were collected for 1 hour, 2 hours, 4 hours and 8 hours after the start of the reaction on GaN substrates. (See Figure 2.11). After 1 hour, the pyramid-shaped ZnO formed. This morphology was reported in [94] where more than 6 hours were needed to form these structures without UV illumination. It indicated that UV illumination increased the growth speed for the reaction. After 2 hours, however, the pyramid-shaped structure changed into nanocones. This can be understood by the absorption process of photons. From figure 2.7 we saw that the solution is not transparent to UV illumination. 70 % of the light was adsorbed. On the other hand, the GaN substrate also strongly absorbs the light with energy larger than its band gap. Thus the solution is directly heated by the UV light and heated from below by the substrate. The light is primarily transformed into thermal energy once adsorbed. Consequently, the local temperature of the solution near the substrate is higher than the temperature of the solution away from the substrate. A thermometer was used to measure the temperature near the reaction surface. The temperature difference between the substrate and the bottom of the solution was about 3℃. Thus the UV light modified the heat distribution as well as the reagent transport. And the a-axis growth speed near the substrate is faster than near the top of the nanostructure so the nanocone morphology is formed. And the overall growth speed was also improved by the UV illumination.

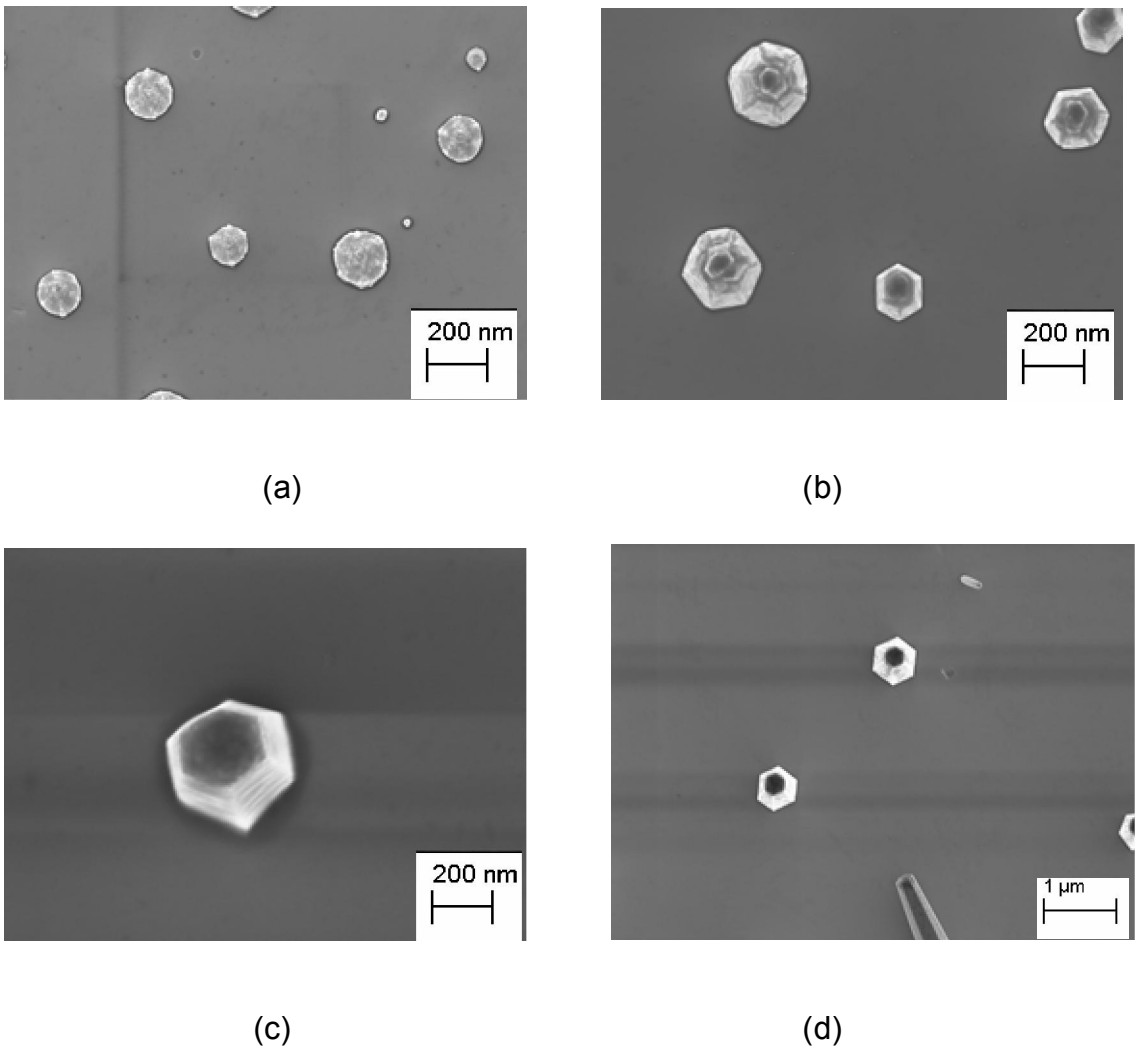

Figure 2.11: SEM pictures for ZnO nanocones taken (a) 1 hour, (b) 2 hours, (c) 4 hours, and (d) 8 hours after the start of the reaction on GaN substrate.

As to the growth process of ZnO nanowires, the lateral growth and axial growth are the same and the morphology will not be changed at the final growth stage, 6 to 48 hours after the beginning of the reaction process [94]. It is not the case for the growth of nanocones (See Figure 2.12). Figure 2.12 shows SEM images taken after 12 hours of growth. The nanocones had turned back to the nanowires by this time, and the beaker was covered with a thick ZnO film formed

in the solution. Thus the UV light was completely blocked. The effect of UV illumination then disappeared and the growth process return to the process of ZnO nanowires.

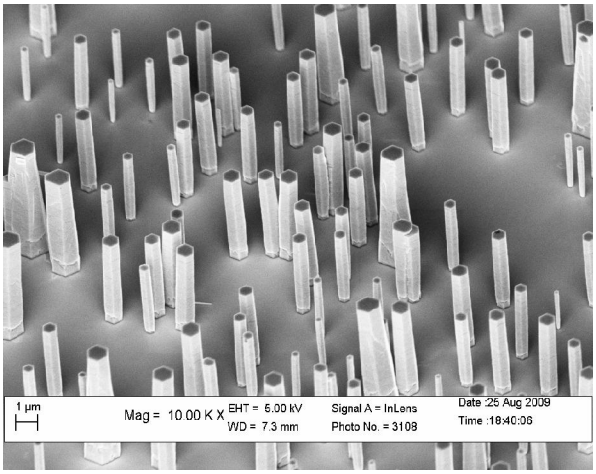

Figure 2.12: SEM pictures for the growth process after 12 hours. ZnO nanocones changed back to nanowires since the whole beaker was covered with a thick ZnO film formed in this process and consequently the UV light was completely blocked.

Although ZnO nanocones turned back to nanowires when the UV light was blocked, it enabled us to analysis the influence of UV illumination on the nucleation process. Figure 2.13 clearly shows that the density of ZnO nanowires was dramatically increased by UV illumination compared to the samples obtained without illumination. This can be understood by the kinetics of nucleation. In the nucleation process, the free energy change is $\Delta G_V = G_V^L - G_V^S$, where G_V^L and G_V^S are the free energies per unit volume of liquid and solid respectively. And $\gamma_{s/l}$ is the solid/liquid interfacial free energy. The free energy change associated with the formation of a small volume of solid has a negative contribution due to the lower free energy of a bulk solid, but there is also a positive contribution due to

the creation of a solid/liquid interface. The creation of small particles of solid always leads to a free energy increase. Thus a nucleation barrier exists for every nucleation process. In addition, stain energy also will increase the nucleation barrier. However, when the chemical reaction system was illuminated by UV light, photons absorbed by the system raised the thermal energy. Thus it is easier for the atoms to overcome the nucleation barrier and more nuclei will be formed, resulting in denser ZnO nanowires.

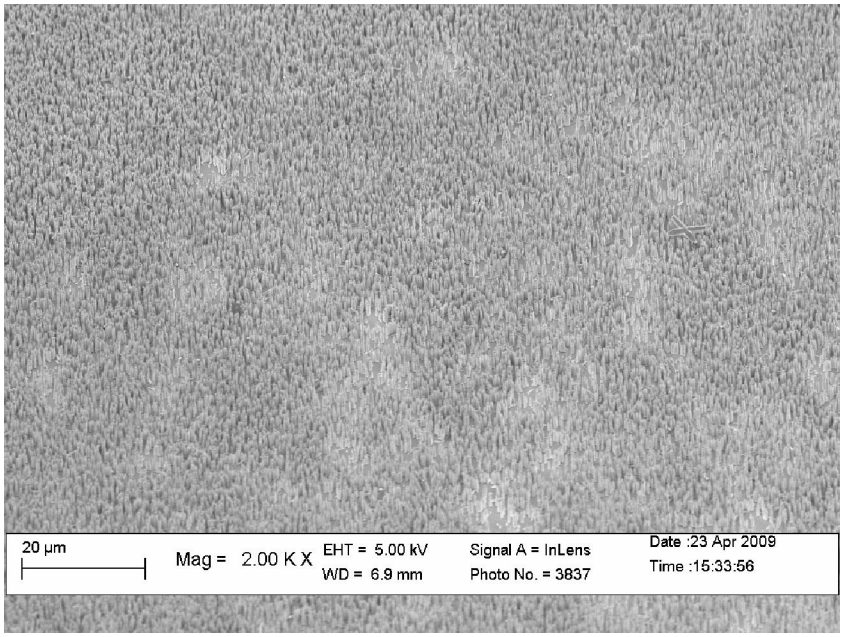

(a)

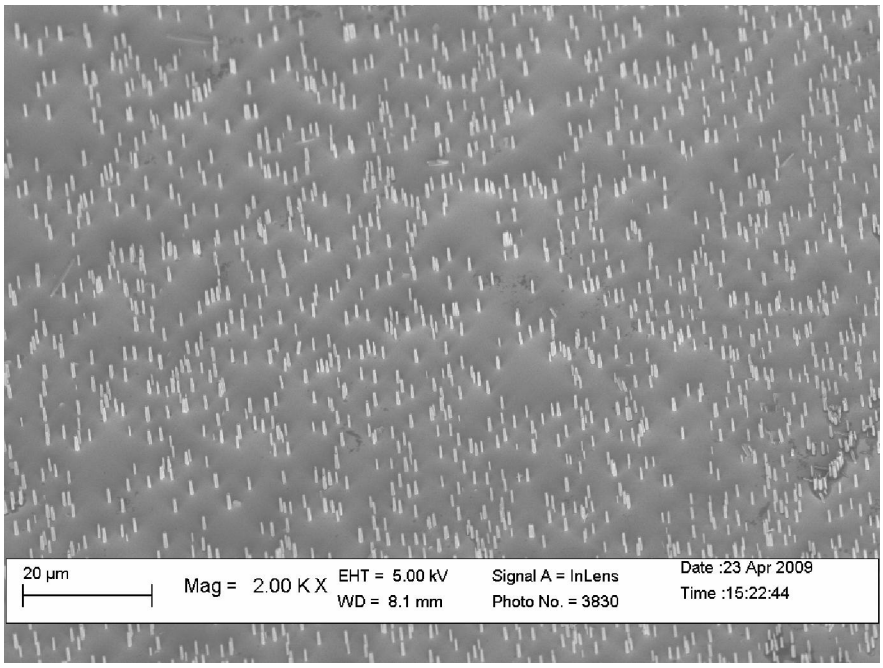

(b)

Figure 2.13 SEM pictures for ZnO nanowires obtained (a) with UV illumination (b) without UV illumination. The density was increased by UV illumination.

Chapter 3

Synthesis of ZnO Nanoplatelets and Characterization

3.1 Background

While an increasing number of papers have been published on the synthesis of one-dimensional ZnO nanostructures, two-dimensional nano or microstructures have not been widely studied due to the lack of knowledge on their synthesis.

ZnO nanosheets or platelets have a great importance for fabricating functional nanodevices due to their high surface to volume ratios, nanometer-scale thickness, interesting optical and photocatalytic activities [107]-[108]. They are expected to be used in energy storage or conversion, data storage, memory devices and optoelectronic fields to further improve the performance of these devices. Ye et al. [109] reported that ZnO nanoplates show good photocatalytic activity and the performance could be improved by thinner nanoplates. These phenomena indicated that c planes have higher photocatalytic activity than the other surfaces of ZnO. Recently, high efficiency dye-sensitized solar cells (DSSCs) were fabricated using ZnO nanosheet electrodes [110]-[111]. High surface to volume ratios enable high dye adsorption, resulting in increased light

harvesting. In this type of DSSCs, conversion efficiency ŋ of up to 3.9% can be achieved.

Various approaches have been utilized to synthesize these 2D ZnO nanostructures such as a vapor transport process [112]-[113], thermal evaporation [114], carbothermal reduction process [115]-[117], chemical bath deposition and a hydrothermal method [118]-[119]. These methods either incorporate high temperature and severe conditions, or complicated procedures and they had difficulties in controllability and repeatability. In addition, the nanoplates or nanosheets obtained are normally intertwined with each other and the thickness of most of these plates is greater than 100 nm. The polar surfaces of these nanoplates are not clean and are always covered with small particles (See figure 3.1 [120]).

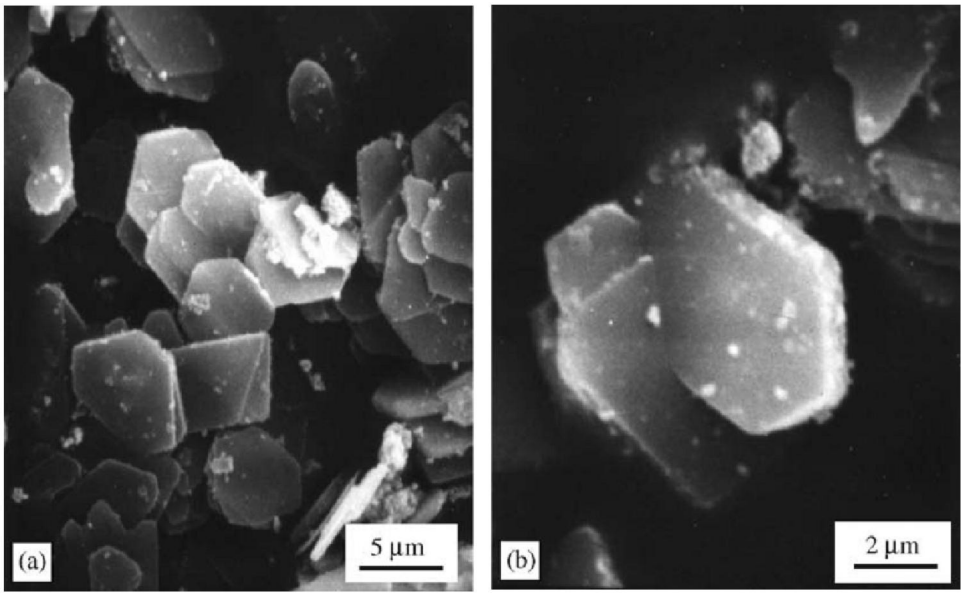

Figure 3.1: ZnO micro-platelets with hexagonal morphologies synthesized by a precursor-growth-pyrolysis approach [120].

The goal of this section is to find an easy way to obtain on a large scale ZnO platelets with clean surfaces and high yield, and use several techniques to characterize these structures.

3.2 Experiment Setup

ZnO nanowires can be synthesized on a GaN film whose c-axis is perpendicular to the substrate [94]. To grow ZnO platelets, however, we need a GaN film whose a-axis is vertical to the surface of the substrate. This requirement can be fulfilled by a new technique with the aid of pulsed laser deposition (PLD) [121].

A Si (0 0 1) wafer of about $2 \times 2\ cm^2$ with a native surface oxide was first cleaned by the standard cleaning process and then was mounted on the sample stage inside the PLD chamber. Both ZnO and GaN targets were mounted so that they could be ablated in sequence without breaking the vacuum. Then the PLD chamber was pumped to the base pressure in the 10^{-7} torr range.

The first step is to deposit ZnO with a texture of [1 0 0] and a thickness of ~100 nm. This can be achieved by ablating the ZnO target with a KrF UV laser ($\lambda = 248\ nm$) in a vacuum of the ~ 1×10^{-6} torr range. In Dr. Hong's paper [120], he investigated the diffraction pattern of textured ZnO deposited by PLD as a function of laser fluencies (See Figure 3.1[121]). The laser pulse power he used

was tuned from 40 to 450 mJ/pulse and the pulses were shot at a fixed rate of 30 Hz to the target surface. Since the beam could be focused to achieve a spot size of $1 \times 1\, mm$, the laser fluence could range from 2 to 45 J cm^{-2}. This result shows that a ZnO texture of [100] could be obtained when the pulse energy is above 35 J cm^{-2}(See figure 3.2). For this experiment, we used 40 J cm^{-2} to get a [100] ZnO texture [121]. This ZnO works as a scaffold for the next stage of GaN growth.

Secondly, the chamber was filled with approximately 2 mtorr of Ar and a substrate heated to approximately 900 ℃. Then the Ar pressure was increased up to ~ 2 torr and the PLD deposition of GaN started as soon as ammonia (NH_3) flowed into the chamber. The frequency of the laser pulses was 5 Hz and the total pressure during the deposition was maintained at ~ 7 torr. Therefore, at high temperature the GaN deposition and the reaction of NH_3 molecules with ZnO occur simultaneously [121].This deposition can last from half an hour to 1 hour, depending on the thickness of GaN desired.

The nutrient solution is also the same as we used for the synthesis of ZnO nanowires [94]. A 1:1 ratio of zinc nitrate and hexamethylenetetramine (HMTA) was dissolved in de-ionized water. However, the concentration of the solution needs to be optimized. In our experiment, the optimal concentration is about 5 mMol/L. Either higher or lower concentration will lead to thick ZnO nanorods or small nanoplatelets. The substrates were up-side-down and floated on the top of the reaction surface. The reaction system was then put in an oven and heated to

85℃. The optimal growth time was less than 5 hours, depending on the thickness desired. Finally the sample was blown dry with nitrogen gas.

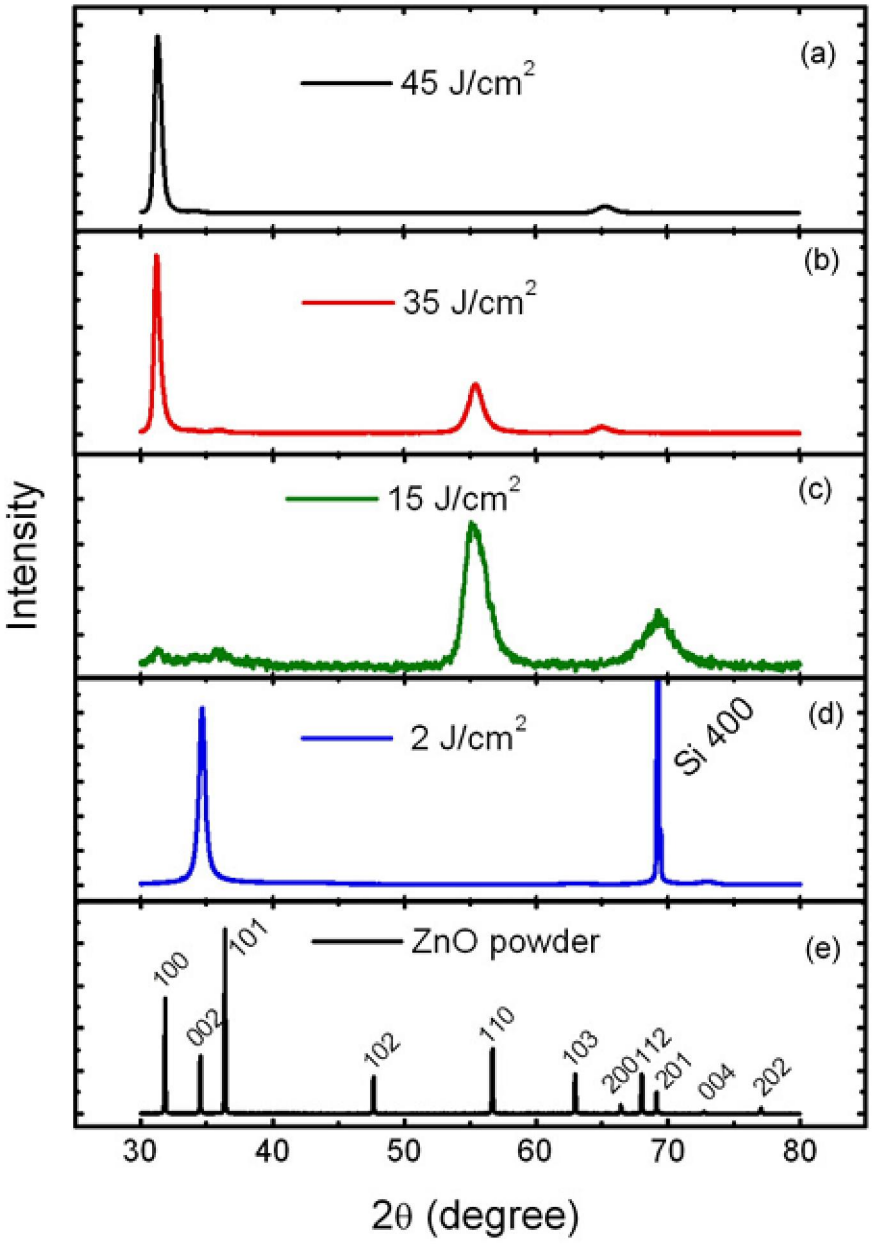

Figure 3.2: X-Ray diffraction pattern for ZnO films obtained at laser fluences of (a) 45 J cm $^{-2}$, (b) 35 J cm $^{-2}$, (c) 15 J cm $^{-2}$, (d) 2 J cm $^{-2}$, and (e) ZnO target [122].

3.3 Experiment Results

A typical SEM image for the morphology of the textured ZnO film deposited by PLD was recorded in [122] (See Figure 3.3). This image shows that the surface of ZnO film is very rough.

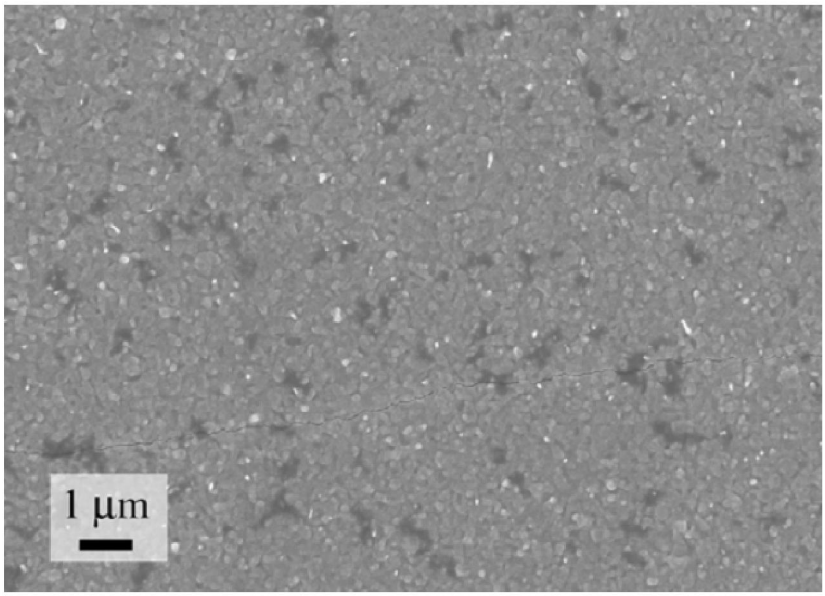

Figure 3.3: Typical SEM image showing the morphology of the textured ZnO film deposited by PLD [122].

We then examined the surface morphology of the GaN film (See Figure 3.4). Crystalline facets were clearly observed and the grain size varies from 100 to 300 nm. The energy dispersive x-ray spectrum (EDS) was also obtained at multiple spots on the sample. (See Figure 3.5). The spectrum clearly indicates that GaN was formed on the silicon substrate. It is very interesting to notice that the peak of Zn does not show up in the EDS spectrum at any area of the film

surface, indicating that ZnO layer was removed completely during the deposition process of GaN.

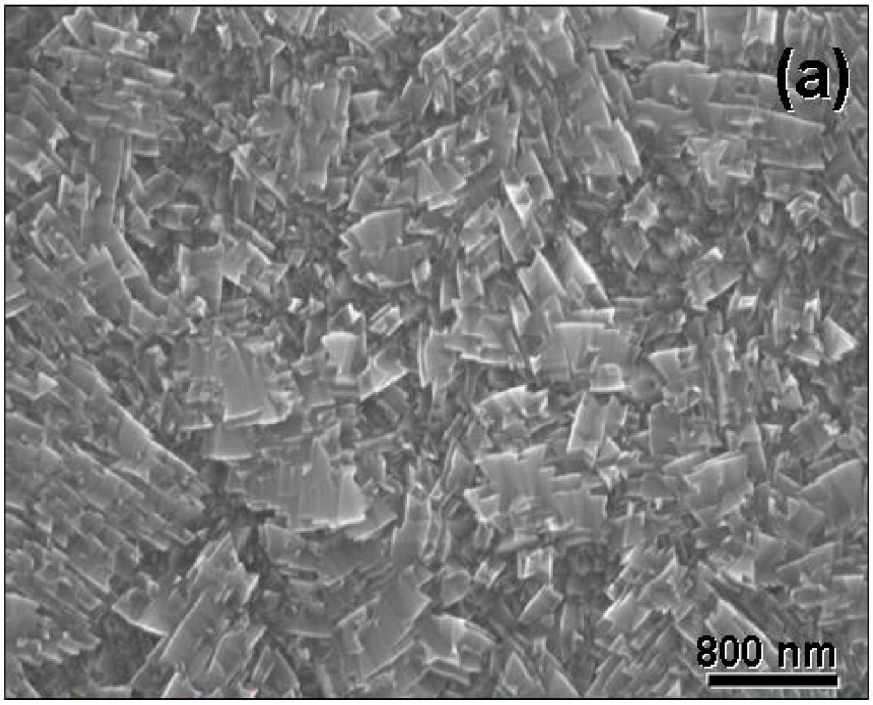

Figure 3.4: The surface morphology of GaN film deposited by PLD

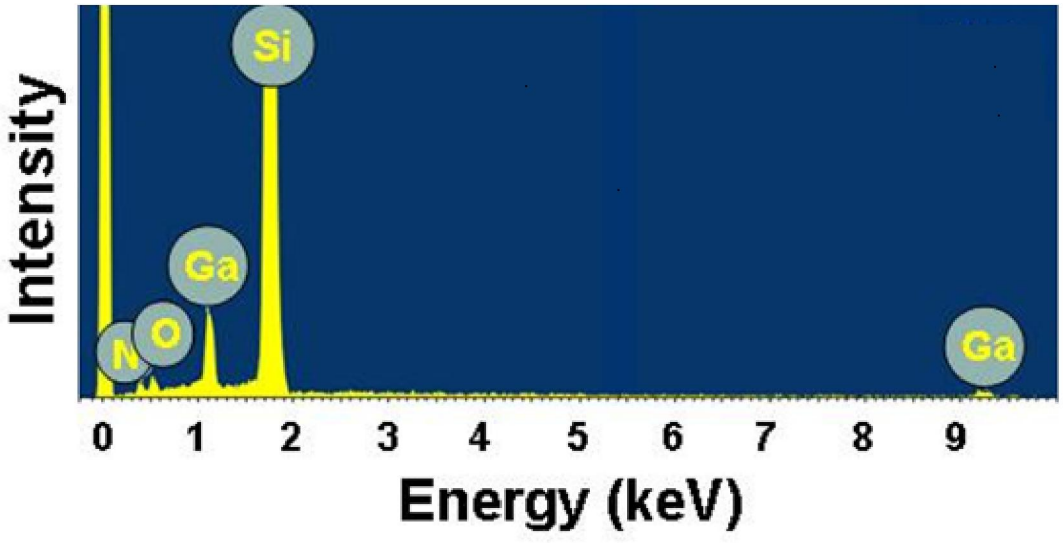

Figure 3.5: The EDS spectrum for GaN film deposited by PLD

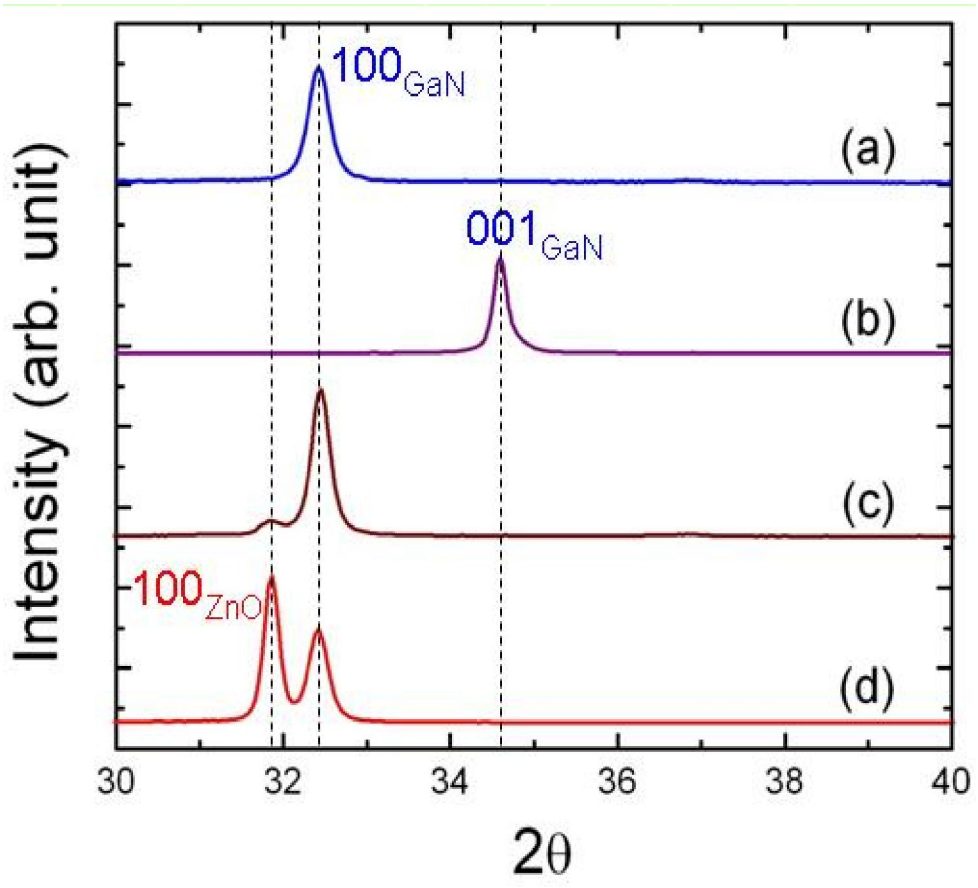

Figure 3.6: X-Ray diffraction pattern for GaN film deposited by PLD. (a) GaN film textured in [1 0 0] direction, (b) GaN film textured in [0 0 1] direction, (c) texture GaN film of [1 0 0] deposited on thick ZnO film, (d) texture GaN film of [1 0 0] deposited on very thick ZnO film[121].

X-Ray diffraction patterns were also obtained for a GaN film deposited by PLD (See Figure 3.6). These results show that GaN films textured in the [1 0 0] and [0 0 1] directions were obtained by controlling the texture of ZnO film deposited in the first step. If the ZnO film is thin, no ZnO peak was observed in this pattern, which corresponded well to the EDS result above. However, a ZnO peak will show up if the ZnO film is thick as shown in figure 3.6 (c) and (d) which

also shows that the intensity of the ZnO peak is proportional to the amount of residual ZnO layer. Therefore, in order to get pure GaN films on a silicon substrate, the thickness of ZnO film deposited in the first step cannot exceed a certain value. In other words, there exists an upper boundary for the thickness of the ZnO film, beyond which ZnO films cannot be removed completely by the reaction with NH_3. The speed of the reaction of ZnO and NH_3 and the deposition rate of GaN are in dynamic balance.

Cross-sectional transmission electron microscopy (TEM) was used to investigate the interface between the GaN film and the silicon substrate in detail (See Figure 3.7). Figure 3.7 (a) shows that there is no sharp and abrupt interface between GaN and silicon. Instead, a ~ 50 nm thick amorphous layer with occasional pores could be observed between GaN film and Silicon substrate with the aid of high resolution TEM (HRTEM) (Figure 3.7 (b) and (c)). Since no other elements were revealed by EDS spectrum, this amorphous interface layer is recognized as SiO_2 or amorphous Ga oxide, or a mixture of both. The existence of a porous and amorphous interface layer can improve the robustness of the deposited film, because usually there is a thermal mismatch between GaN and Silicon [121]. A fringe image of GaN grains shown in Figure 3.7 (c) indicates the good crystal quality of the GaN film. Figure 3.7 (d)-(f) are the plane-view TEM images of the GaN film. The electron diffraction pattern shown in figure 3.7 (d) confirms the [1 0 0] texture of the film. The set of {1 0 0} and {1 0 1} rings are negligible compared to the strong intensity of {0 0 2} diffraction ring, which indicates that the c-axis of the GaN film are mostly parallel to the surface,

although they are are randomly distributed within the film plane. SAED pattern was also obtained from a grain marked in the middle of figure 3.7 (e). Combined with the HRTEM image of the same area, it is clear that c-axis lines within the film surface.

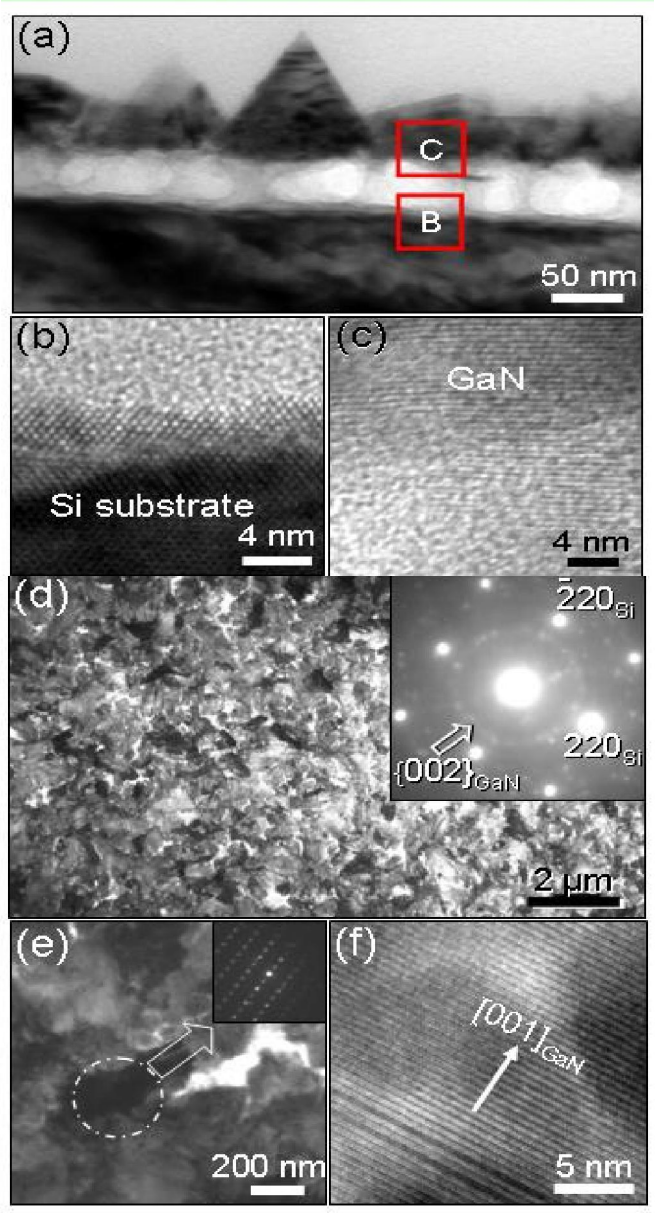

Figure 3.7: (a) Cross-sectional TEM images of the interface between the substrate and GaN film. (b) and (c) are HRTEM images at the interface area of Si substrate, and GaN film. (d) Plan view and ED pattern (inset) of [100] textured GaN film. (e) and (f) are SAED pattern and HRTEM image of one of the grain, respectively [121].

The general morphologies of as-grown ZnO platelets on GaN films were examined by scanning electron microscopy. Low, medium and high magnification images of hexagonal-shaped ZnO platelets are shown in figure 3.8. Low-magnification images reveal that numerous random distributed nanoplates formed on the whole GaN film, implying that this chemical approach has wide application in the fabrication of large-scale nanoplates. Unlike the results from a majority of related papers, these ZnO nanostructures are not closely intertwined with each other. Individual ZnO platelets could be picked up to fabricate a single ZnO platelet device. The average dimensions of the observed ZnO platelet are in the range of 2-5 μm with the typical thickness of 20-50 nm and they are almost perpendicular to the substrate. These platelets are connected to the GaN film and some of them only have half the hexagonal shape. The surfaces are clean and no particles were observed on the platelets.

Further detailed structural characterization of the ZnO platelets was performed using transmission electron microscopy (TEM) combined with the selected area electron diffraction (SAED) pattern. Figure 3.9 shows the low magnification and high resolution TEM images of the fragment ZnO platelet dispersed from the substrate. The hexagonal-shaped morphology of the ZnO platelet is also confirmed by TEM images. The corresponding SAED pattern of the fragment of the ZnO platelet illustrates that the obtained ZnO platelets are single crystalline grown along the <0 1 $\bar{1}$ 0> direction within the {0 0 0 1} planes. The HRTEM image of the ZnO platelets shows that the distance between two lattice fringes is about 0.52 nm, corresponding to the (0 0 0 1) crystal planes of

ZnO. In addition, there is also one or two atomic amorphous layer on top of ZnO platelet due to the low temperature growth.

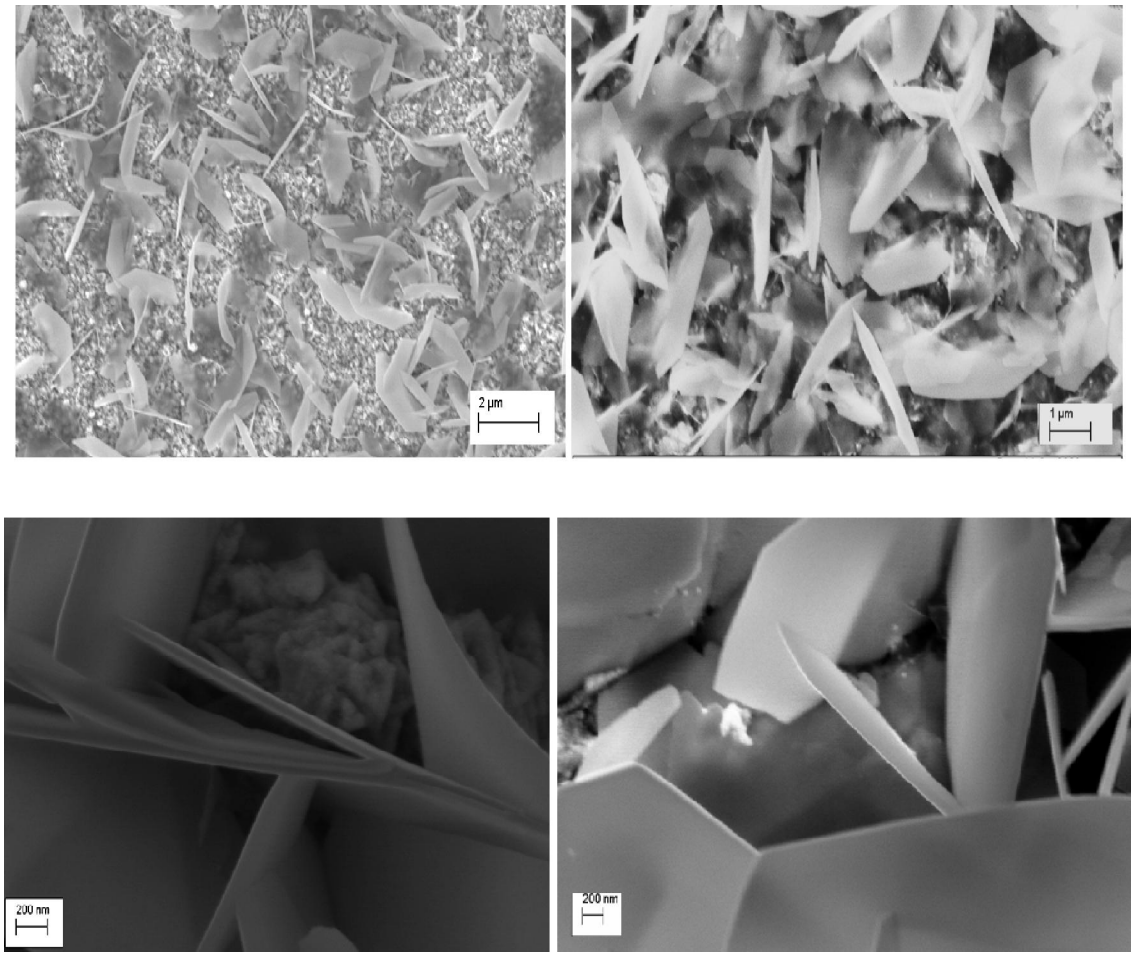

Figure 3.8: SEM pictures of different magnification for ZnO platelets synthesized on GaN film whose c-axis is lying within the film plane.

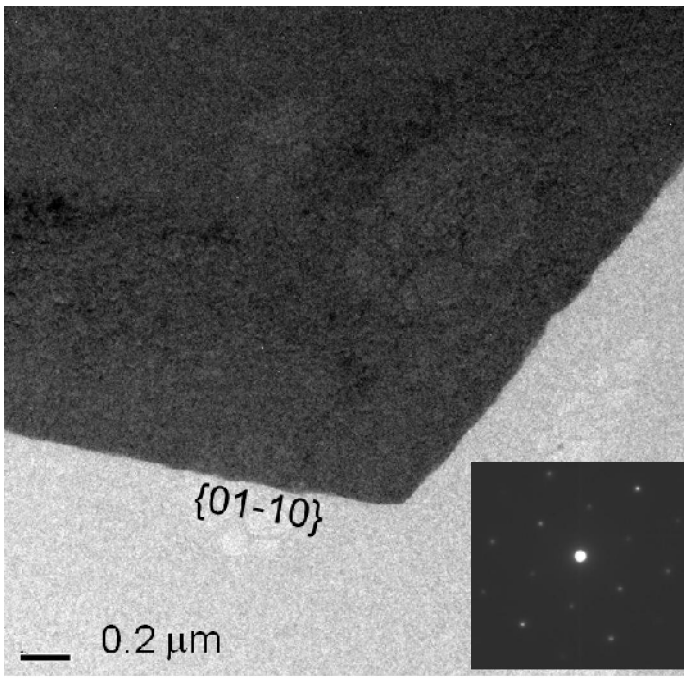

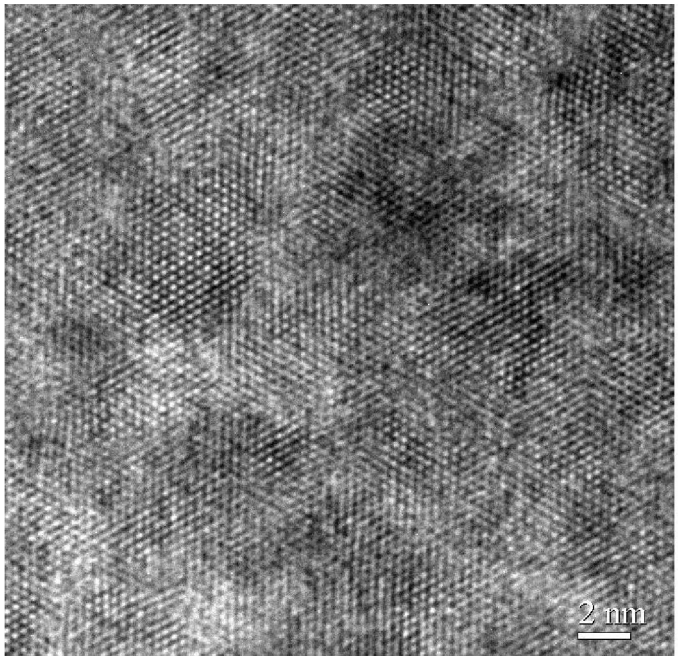

(b)

Figure 3.9: (a) the low magnification and (b) high resolution TEM images of the fragment ZnO platelet dispersed from the substrate. Inset is the SAED pattern for ZnO platelet.

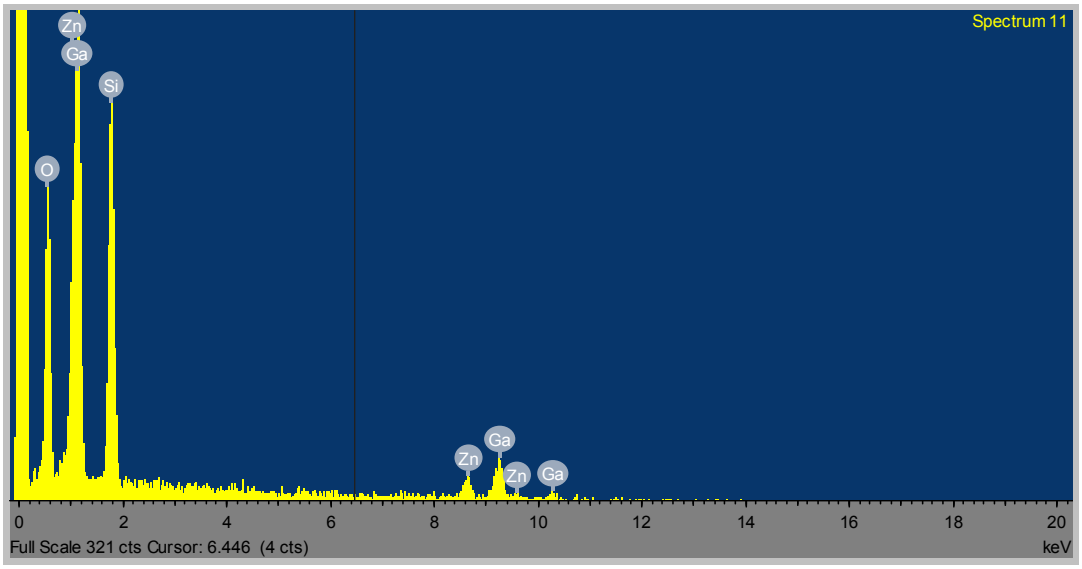

Figure 3.10: EDS spectrum for as-grown ZnO platelets on GaN film.

An EDS spectrum (See figure 3.10) was taken to identify the chemical composition of the ZnO platelets. The result shows that no contamination was involved within this sensitivity of EDS. ZnO platelets were well formed on the GaN film by this catalyst free chemical method, where the substrate is silicon.

3.4 Discussion

3.4.1 Growth Mechanism

A ZnO crystal is composed of a polar top surface, a polar basal plane {0 0 0 1} and a nonpolar plane (0 1 $\bar{1}$ 0) and (2 $\bar{1}$ $\bar{1}$ 0) with C_{6v} symmetry. The low-symmetry, nonpolar face is the most stable with its 3-fold coordinated atoms, while the polar faces are metastable and possess higher surface energy as compared to the nonpolar face. Under thermodynamic equilibrium conditions the higher surface energy facet has a smaller area, while the lower surface energy has a larger area. Therefore, the overall surface energy is minimized. Correspondingly, the relative growth rates of various crystal facets lead to different growth behavior. Under hydrothermal condition, the growth velocities of the ZnO crystals are $V_{<0\,0\,0\,1>} > V_{<0\,1\,\bar{1}\,0>}$ [123]. Therefore, growth along the c-axis [0 0 0 1] direction is the typical growth behavior of ZnO nanostructures, resulting in nanowire or nanorod type morphologies.

However, regarding the growth of ZnO platelets, relative growth rates of various facets were altered by the presence of the [1 0 0] textured GaN film. We suppose that the growth in the [0 0 0 1] direction is strongly suppressed by [1 0 0] textured GaN film and so it grows along the six directions <0 1 $\bar{1}$ 0>. Thus, the continuous growth in six <0 1 $\bar{1}$ 0> directions leads to the formation of hexagonal platelets. Traditionally, the suppression of the growth along +c axis can be achieved by citrate anions, as a structure-directing agent, adsorbing selectively on the ZnO basal planes [124]. In the present case, the suppression effect is

likely to originate from the stress applied by the [1 0 0] textured GaN film on the ZnO nuclei. However, to precisely understand the detailed growth process for the formation of ZnO platelets, further study is needed.

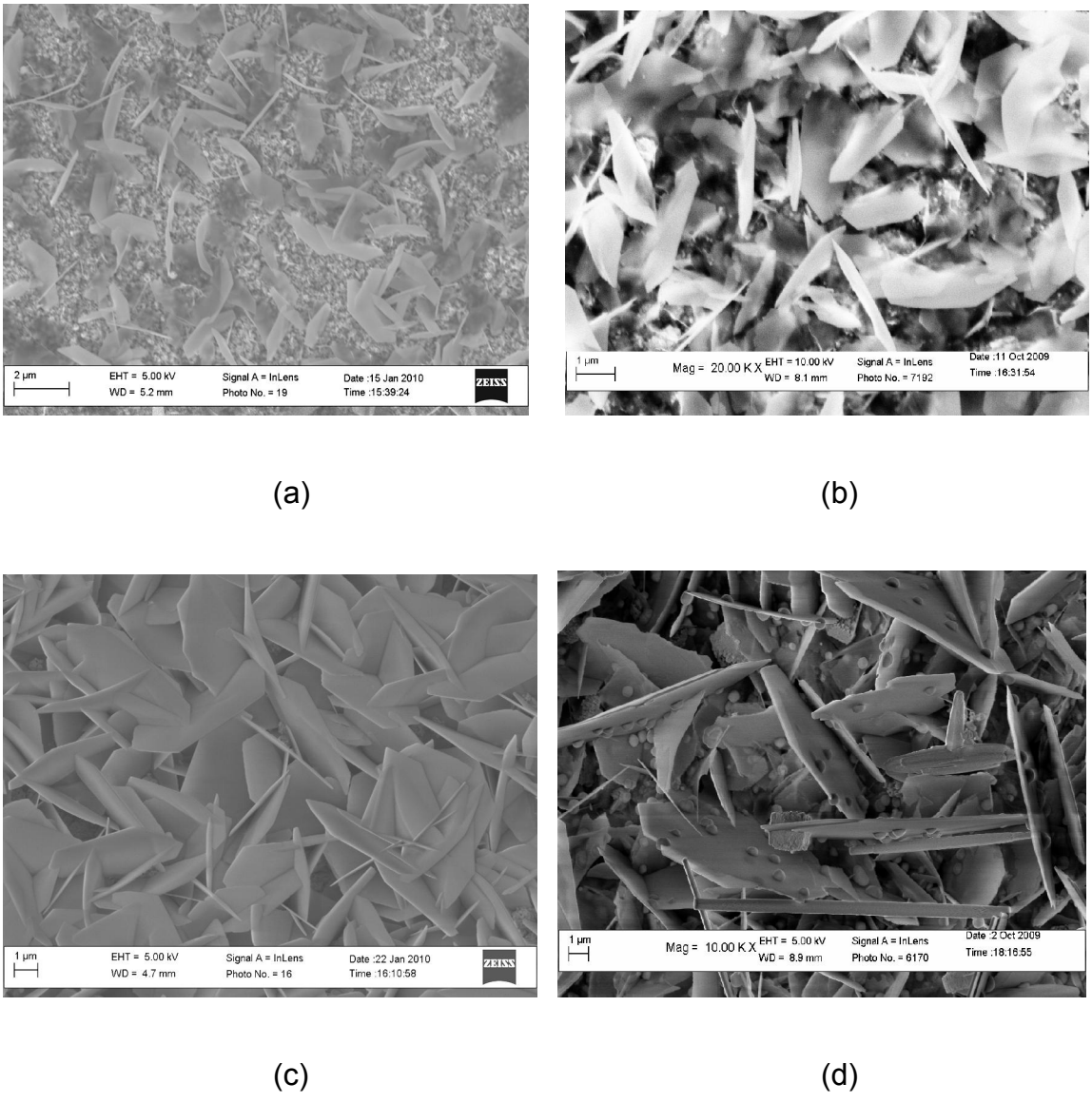

Figure 3.11: SEM images for ZnO platelets obtained after growth times of (a) 1 hour, (b) 3 hours, (c) 5 hours, (d) 14 hours.

In order to further investigate the growth mechanism, we studied the time dependence of the growth of ZnO platelets. SEM images were taken for ZnO platelets grown for 1 hour, 3 hours, 5 hours and 14 hours. (See Figure 3.11). These pictures show that the time for the formation of ZnO platelets is short compared to ZnO nanowires. Usually for ZnO nanowires, only some very small particles can form within 1 hour. It is not the case for the growth of ZnO platelets. After 1 hour, small ZnO platelets have formed with diameters up to 1 μm. It is also worthy to notice that growth along c-axis is strongly suppressed during this growth process. From 1 hour to 3 hour, the thickness variation is negligible compared to the increases in diameter. Thicker platelets could be obtained after 5 hours with larger diameters. However, the diameter of ZnO platelets cannot be increased simply by extending the growth time. After 14 hours, small particles will form on the surface of ZnO platelets. The top and bottom surface of the ZnO platelets are polar surfaces and possess high surface energy and they are an ideal place for secondary growth of other ZnO nanostructures as figure 3.11 (d) shows.

Conventionally, citrate anions are used as structure-directing agents to adsorb selectively on ZnO basal planes so that the growth along +c axis can be suppressed [124]. Following this idea, 0.02 mMol/L of sodium citrate was dissolved in the growth solution for comparison. Figure 3.12 displays the SEM pictures for ZnO platelets obtained under the same conditions but (a) without sodium citrate and (b) with sodium citrate. Clearly, the average thickness of sample obtained with sodium citrate is smaller than that of sample without

sodium citrate. The growth along c axis is suppressed by the presence of sodium citrate. These citrate anions attached to the ZnO basal planes so the further movement of Zn^{2+} and O^{2-} towards to the basal planes was blocked. Thus, the morphology is further confined by the sodium citrate.

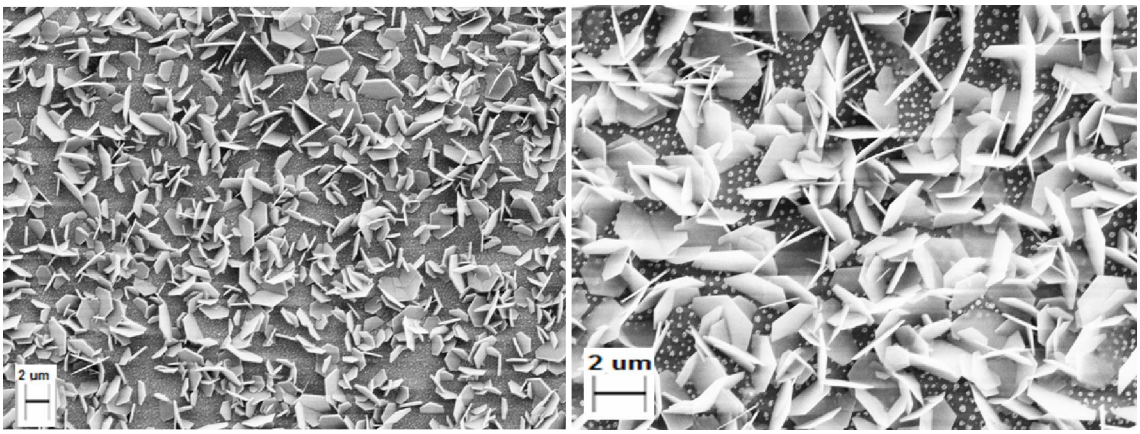

(a) (b)

Figure 3.12: SEM images for ZnO platelets obtained (a) without sodium citrate and (b) with sodium citrate.

It is very interesting to notice that the thickness of the ZnO platelets is also dependent on the thickness of the GaN film. At the edge of GaN film, usually thick ZnO platelets can be found (See Figure 3.13 (a)). In fact, since the GaN film is deposited by the PLD method, the thickness distribution is not uniform. And it is thin or almost disappears at the edge of the sample. The GaN film is either very thin or discontinuous in these areas. In the middle of the sample, on the contrary, the thickness is more uniform and relative thick.

At the edge of the sample, where the GaN film is thin or discontinuous, the thickness of the ZnO platelets could achieve 100 nm or above (See figure 3.13

(b)). In some cases, ZnO nanowires could be observed as well as ZnO platelets. As we proposed above, the stress from GaN film is supposed to suppress the growth along c-axis. However, if the film is too thin or the grain size of GaN film is too small, the stress may not be strong enough to suppress the growth along c-axis. Intrinsically, c-axis growth along the [0 0 0 1] direction is the typical growth behavior of ZnO nanostructures. Thus, two competitive growth mechanisms are involved. ZnO crystals tend to grow along c axis while the stress provided by GaN film wants to confine its growth along c axis. When the stress is small and cannot completely suppress the growth along c axis, thicker platelets are observed. If the silicon substrate is exposed due to the discontinuous deposition of GaN, ZnO nanowires will form as long as these parts of silicon become the nucleation sites for ZnO. In the middle of GaN film, where the GaN film is very thick and the stress is strong, thin platelets are expected and conformed by figure 3.13 (c).

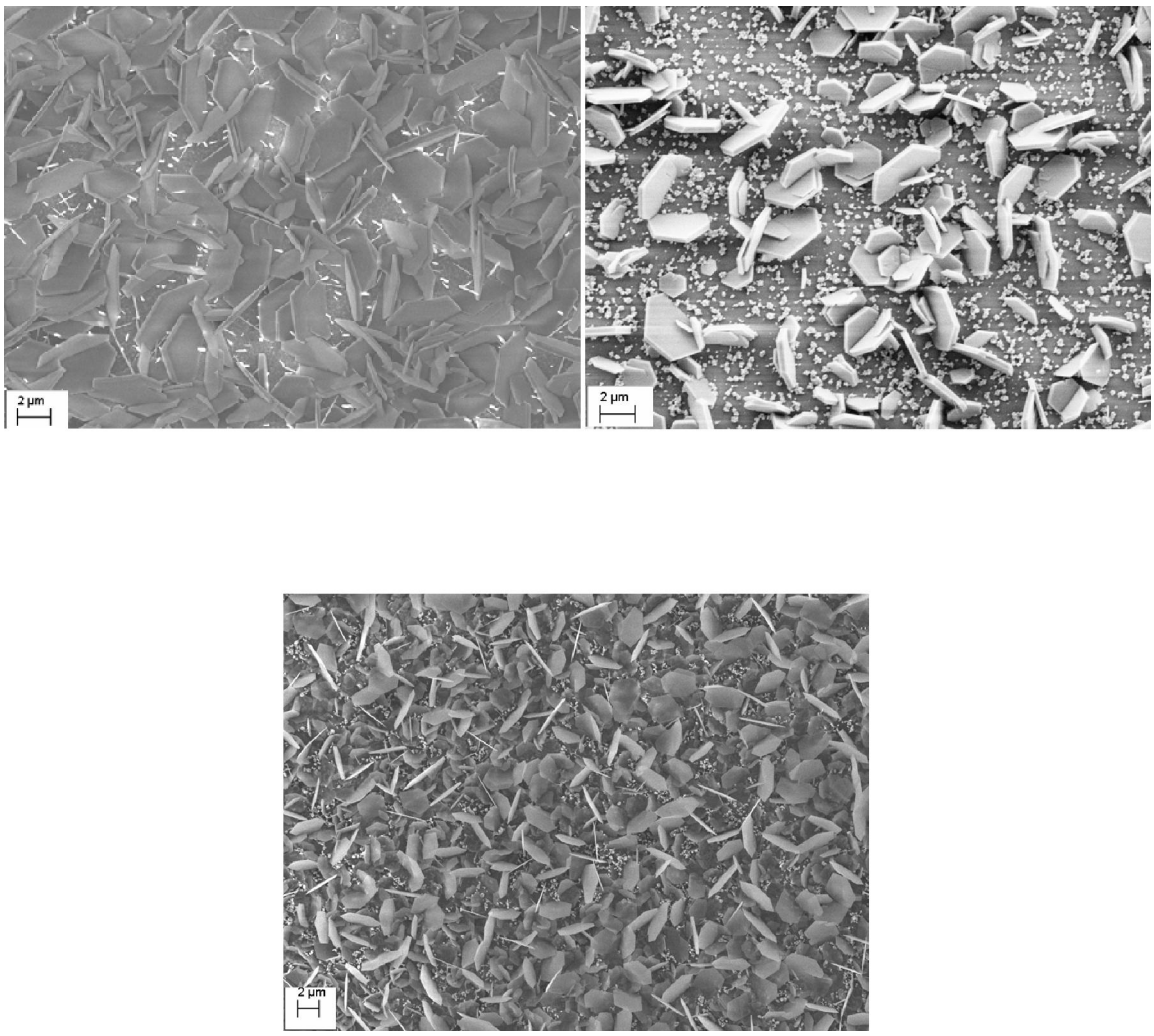

(c)

Figure 3.13: SEM images for ZnO platelets formed on (a) discontinuous GaN film, (b) thin GaN film, and (c) thick GaN film.

3.4.2 Electrical Measurement of ZnO Nanoplatelets

A bigg ZnO platelet (> 15 μm in diameter) is desirable to make single ZnO platelet device since it possess significant surface area and is easier to be manipulated. However, our previous results show that only 5 μm diameter ZnO platelets can be achieved and that a majority of ZnO platelets have diameters ranging from 2 to 4 μm. On the other hand, we showed that the morphology of ZnO platelets also depend on the quality and thickness of GaN film deposited by PLD. Thus, we optimized the growth of GaN films by changing the deposition rate and time. Wide ZnO platelets with 20 µm diameter were thus obtained (See figure 3.14).

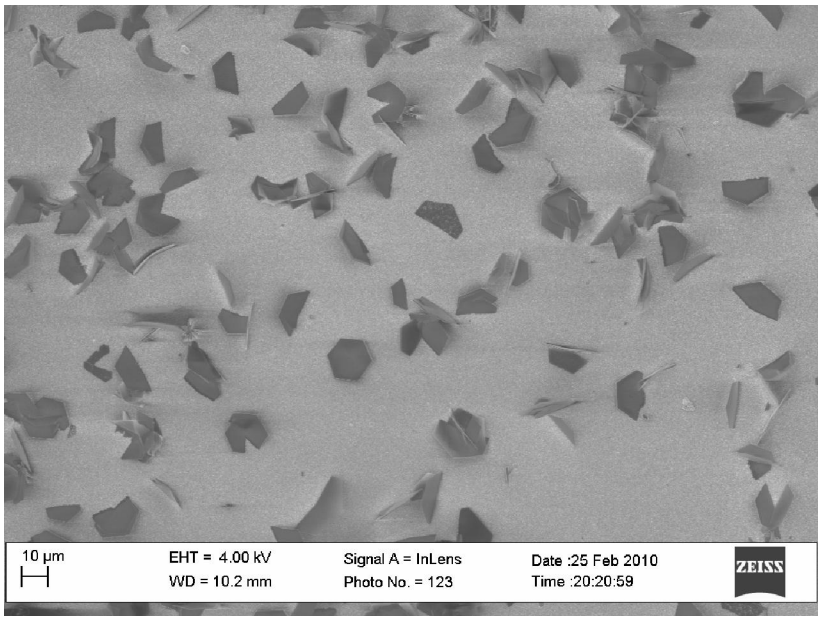

Figure 3.14: SEM images for wide ZnO platelets formed on GaN film.

While it may be technical difficult to control the quality and the thickness of GaN film precisely in an experiment, another approach can be used based on the photolithography process. In our experiment we found that the ZnO platelets tend to intertwine with each other to form a network if the density of ZnO platelets is too high (See Figure 3.15). In this case, the size of the ZnO platelets is also very small. Owing to the high density of nucleation, the space for each platelet is very small and the growth for each individual plate is special confined by the presence of other plates.

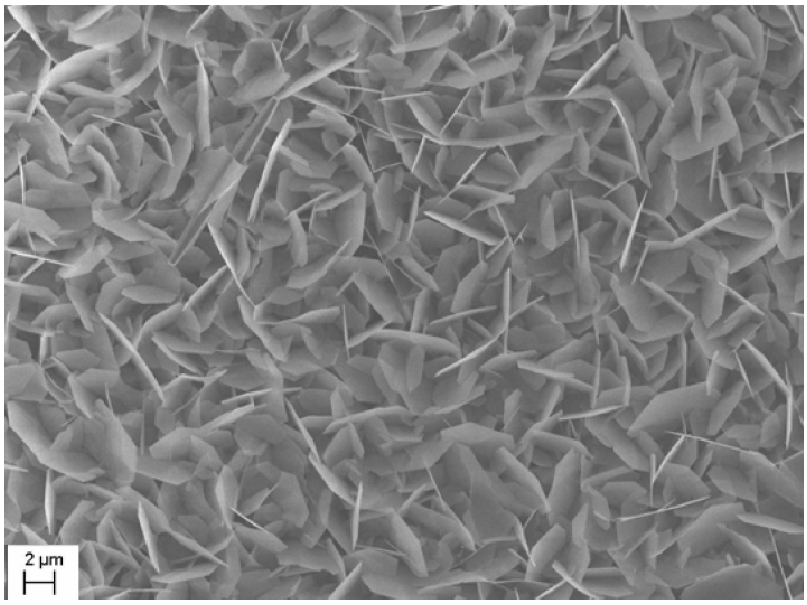

Figure 3.15: SEM images for ZnO platelets that intertwine with each other.

Thus, we patterned the GaN film with 1827 positive photo resist with parallel stripes. The spacing between two parallel stripes is $5\mu m$. The result for

ZnO platelets formed on patterned GaN film can be found in figure 3.16. The platelets grew separately to diameters up to 12 μm.

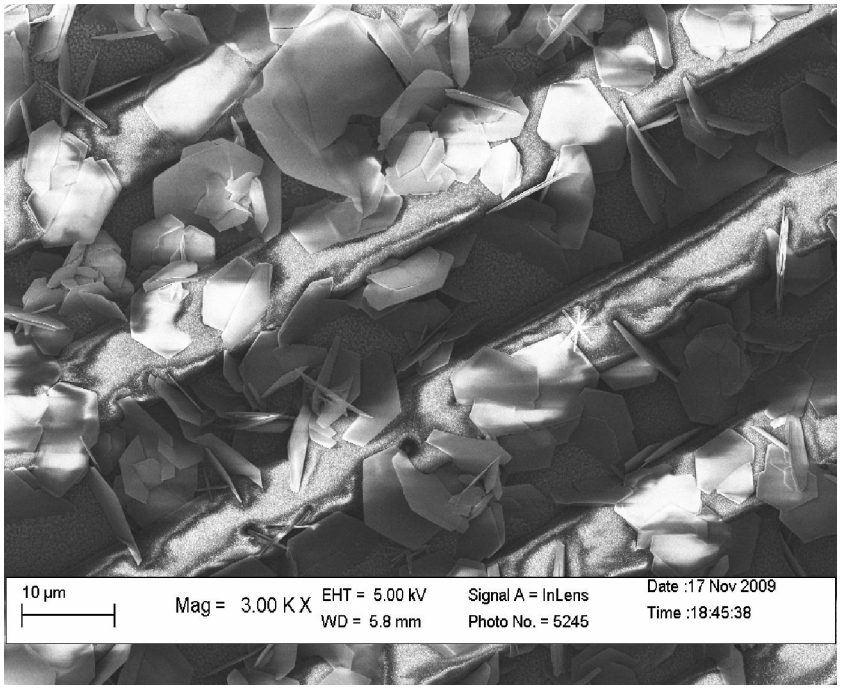

Figure 3.16: SEM images for ZnO platelets on patterned GaN film.

To perform electrical measurements, a single ZnO platelet is bridged between two electrodes. When the metal is attached to the semiconductor material, two kinds of contacts can be formed. The first one is an Ohmic contact where the current-voltage characteristic of the device is linear and symmetric. The second case is Schottky contact where the current-voltage characteristic of the device is non-linear and asymmetric. (See figure 3.17).

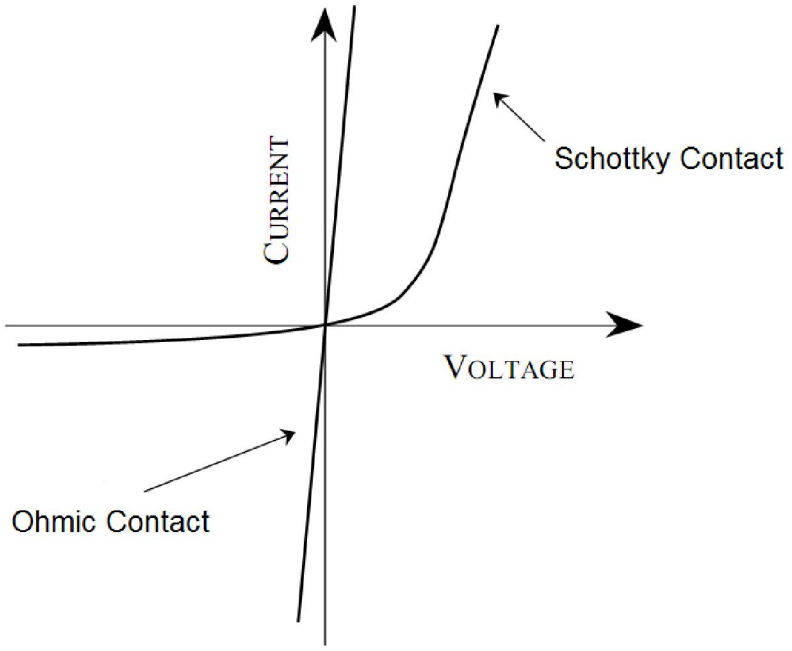

Figure 3.17: I-V characteristic of Ohmic and Schottky contact.

The formation of either an Ohmic contact or a Schottky contact depends on the difference in work functions between metal and semiconductor. Energy band diagrams for ideal metal-n type semiconductor contacts can be found in figure 3.18. Vacuum level E_0 corresponds to the energy of free electrons. The work function Φ of materials is defined as the difference between the vacuum level and Fermi-level. The work function Φ_M is an invariant property of metals and is the minimum energy required to free electrons from a metal. The semiconductor work function Φ_S depends on the doping. $\Phi_S = E_0 - E_{FS}$, where E_0 is the vacuum energy and E_{FS} is the Fermi level. χ is a fundamental property of the semiconductor and $\chi = E_0 - E_C$, where E_C is the lowest energy of the conduction band.

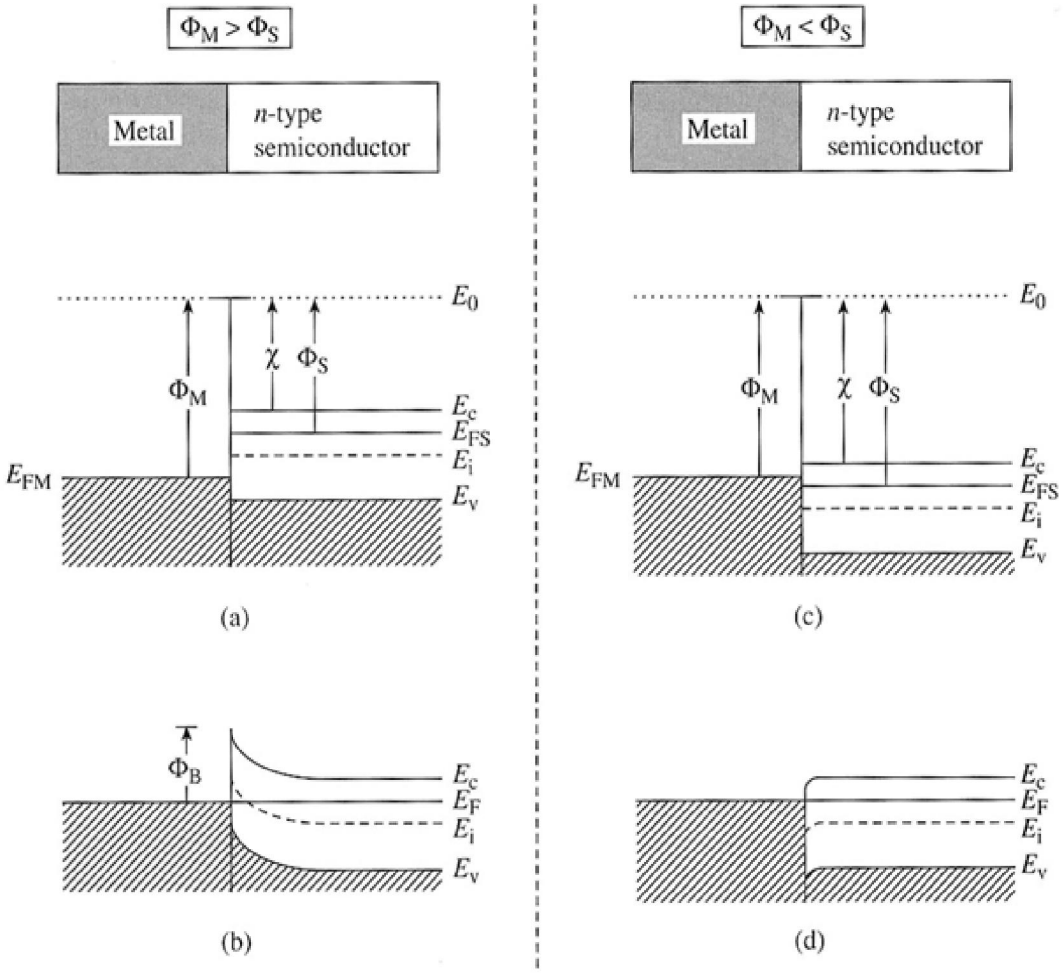

Figure 3.18: band diagrams for ideal metal-semiconductor contacts (a) before contact (b) Schottky contact is formed, (c) before contact and (d) Ohmic contact[125].

The Fermi level of any two solids in contact must be equal in thermal equilibrium. If $\Phi_M > \Phi_S$ for n-type semiconductor when brought into contact with the metal, electrons will begin to flow from the semiconductor to the metal near the junction. Thus a surface depletion layer as well as a built-in electric field will be set up. Semiconductors possess a positive charge while the metal possesses a negative charge near the interface. Under thermal equilibrium, net flow of

carriers will be zero and the Fermi level will be constant. However, electrons moving from metal to semiconductor have to overcome a barrier $\Phi_B = \Phi_M - \chi$. Electrons will encounter an energy barrier equal to $\Phi_M - \Phi_S$ while flowing from semiconductor to metal. A Schottky contact is formed in this case. On the other hand, if $\Phi_M < \Phi_S$ for an n-type semiconductor, there is no barrier for electrons flowing from the semiconductor to the metal and an Ohmic contact is formed. The electrical nature of ideal metal-semiconductor contacts is summarized in table 3.1.

Table 3.1: Electrical nature of ideal metal-semiconductor contacts

	n-type semiconductor	p-type semiconductor
$\Phi_M < \Phi_S$	Ohmic	Schottky
$\Phi_M > \Phi_S$	Schottky	Ohmic

The work function Φ_S of n-type ZnO is 4.53 eV [126]. According to table 3.1 and table 3.2, the junction between n-type ZnO and Au or Pt results in a Schottky contact, while the junction between n-type ZnO and Ti, Ag or Al leads to an Ohmic contact. In our experiment, Au was deposited to fulfill requirements in photolithography.

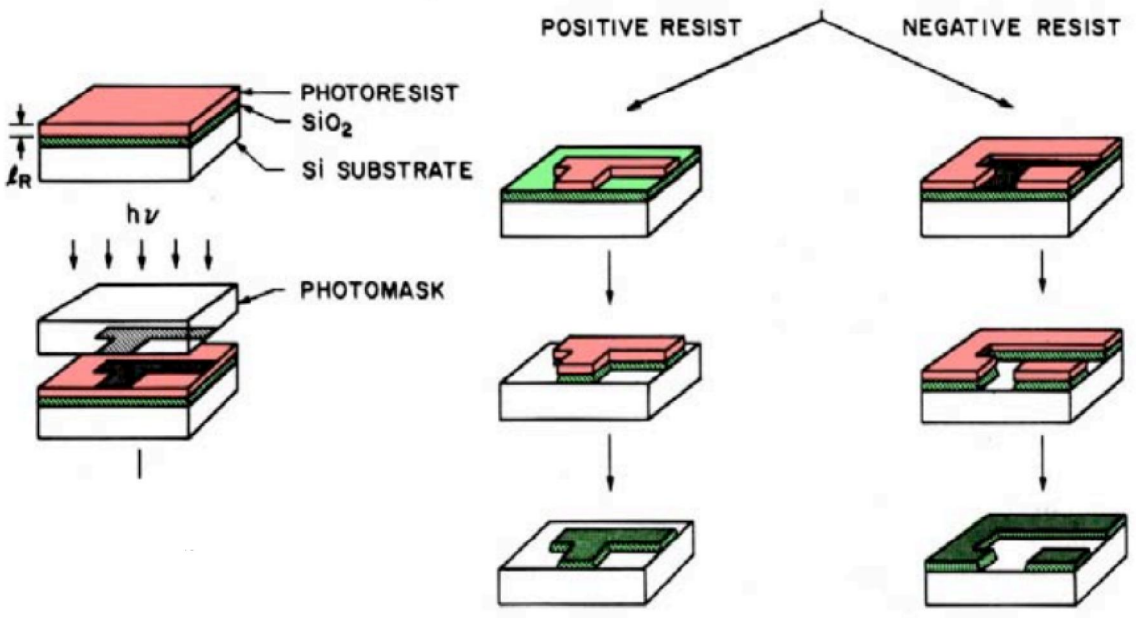

Figure 3.19: Schematic of photolithography process [127].

Since the size of ZnO platelets is very small, we cannot directly deposit metals on the desired spots. Usually this issue can be solved by optical photolithography processes. Photolithography is a process sequence to transfer a layout from a mask to the wafer surface (See Figure 3.19). In brief, the photolithography process begins with the spin coating of a photoresist. The photoresist is soft baked to dry and evaporate solvent around 80 -100 ℃ for 30 seconds. Then we align the mask and wafer and expose the photoresist to UV light with specific wavelength and intensity. The next step is to develop and rinse the non-cross-link photoresist. Finally, a hard bake is applied.

There are two types of photoresist: positive photoresist and negative photoresist. For positive photoresist, exposed areas will be dissolved in the

developer in the development process. Unexposed areas are essentially unchanged by the presence of developer, thus ensuring a better resolution compared to a negative photoresist. For negative photoresists, on the contrary, exposed areas cross-link and become insoluble in the developer. Thus only unexposed areas are removed during development. The main problem for this type of photoresist is that exposed areas always swell during the development process, thus reducing resolution. Positive photoresist is preferred in most cases today.

The electrode we used here is Au. Figure 3.20 shows the schematic of a single ZnO platelet device with two gold electrodes on a silicon oxide substrate. The gap between the two electrodes is $2\mu m$. The average size of our platelet is chosen from 2 to $20\mu m$. However, these as-grown platelets are strongly attached to the GaN film and need to be transferred to the silicon oxide substrate. During this transfer process, the platelets may be broken so the actual size of the platelet may be smaller than this range and the perfect hexagonal shape may not be able to be retained.

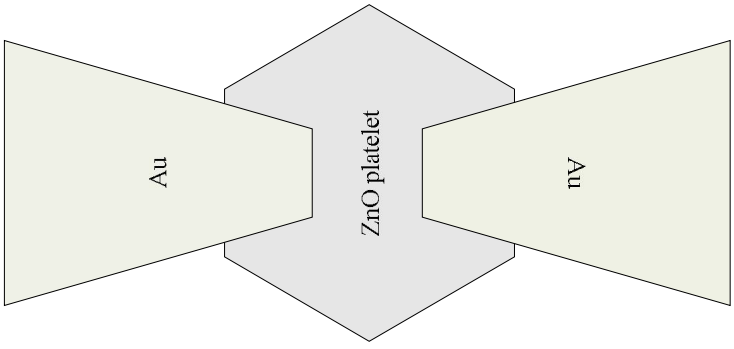

Figure 3.20: Schematic of single ZnO platelet device with two gold electrodes on Silicon oxide substrate.

In practice, ZnO platelets are randomly distributed on the silicon oxide substrate and deposit the gold electrodes by the photolithography process. There is a chance that the two electrodes are directly on top of a single ZnO platelet at the right position. However, in our experiment the yield of this method is quite low. It is much easier to get only one electrode on top of ZnO platelet. The probability of having two electrodes at the right position, however, is significantly reduced.

Thus, we add another step in our experiment to improve the yield. We first deposited a pair of $50 \times 50\,\mu m^2$ of gold arrays on top of the silicon oxide substrate. These big gold electrodes function as markers that can guide us to put the ZnO platelet just between each pair of two big electrodes under an optical microscope. Then the other set of gold electrodes in trapezoid shape like figure 3.20 were deposited just between two big electrodes by a mark aligner. (See figure 3.21). We found that the yield of single ZnO platelet devices is greatly improved by this method.

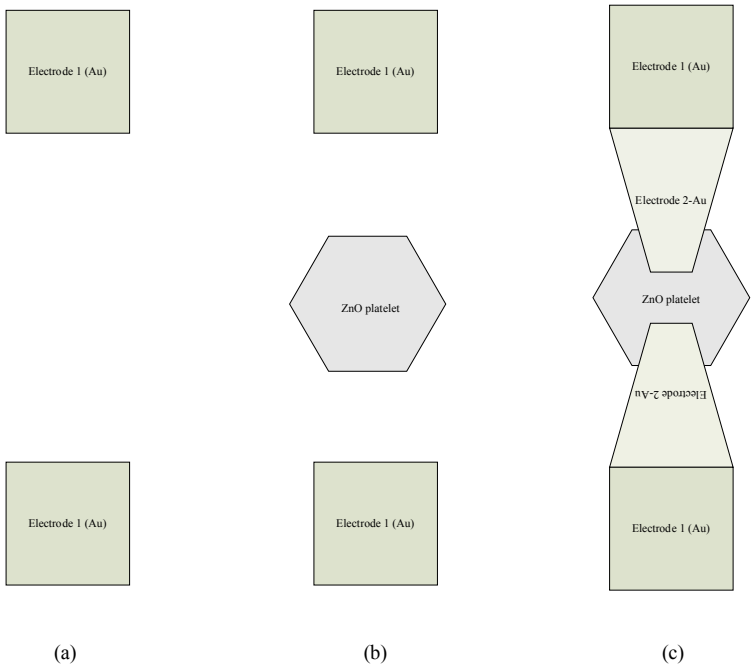

Figure 3.21: process flow to fabricate single ZnO platelet device. (a) Deposit first set of big electrodes, (b) put the ZnO platelet just in the middle of two big electrodes, and (c) deposit the second set of electrodes within the gap of first set of big electrodes.

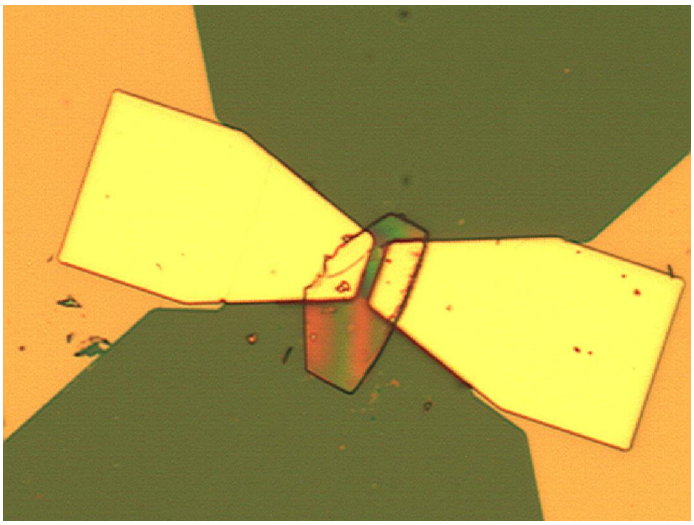

Figure 3.22: optical image of single ZnO platelet device with two Au electrode on Silicon oxide substrate.

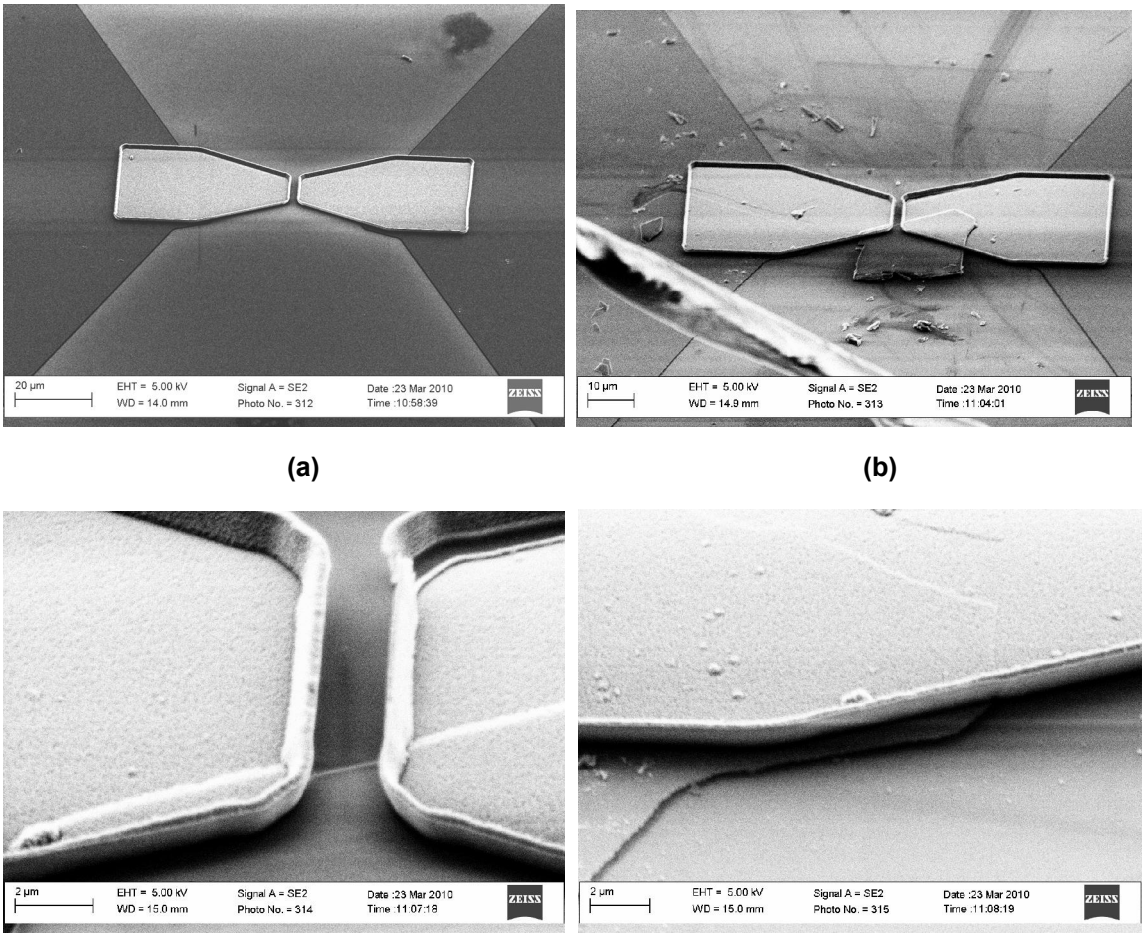

Figure 3.23: (a) SEM image of a pair of electrode without ZnO sample, (b) SEM image of single ZnO platelet device with two gold electrodes, (c) and (d) high magnification SEM image of the details of single ZnO platelet device.

Figure 3.22 is the optical image of a single ZnO platelet device with two gold electrodes on a silicon oxide substrate. As mentioned above, ZnO platelets are fragile and easily get broken when we transfer them from the GaN film. Thus, normally only half of the ZnO platelets appear as in figure 3.22. To further examine the contacts between the ZnO platelet and the gold electrode, SEM images were taken to see the details in the contact area. (See figure 3.23). These images show that the electrodes were well deposited and attached to the

surface of ZnO platelet. The gold electrode on top of ZnO platelet was continuously extended to the big gold electrode without any gaps.

To perform low current measurement, a KEITHLEY 4200 semiconductor characterization system was used. The smallest current it can detect is 1pA with preamplifiers.

The representative current-voltage (I-V) curves of a single as-grown ZnO platelet device are shown in figure 3.24. A majority of ZnO platelets have the non-linear I-V curve as figure 3.24(a) shows, while some of ZnO platelets show linear I-V behavior l like figure 3.24(b). It is statistically dependent on the local contact. The current range is in the pico ampere range when the voltage is smaller than 5 volts. The measured resistance for our ZnO platelet is about 20-40 GΩ. In paper [128], they reported that the resistance for a ZnO nanosheet-nanowire network complex synthesized by polymer-controlled chemical approach is about 163GΩ. Thus, the resistance of our ZnO platelet is smaller than their result but still it is much higher than the resistance of ZnO nanowires.

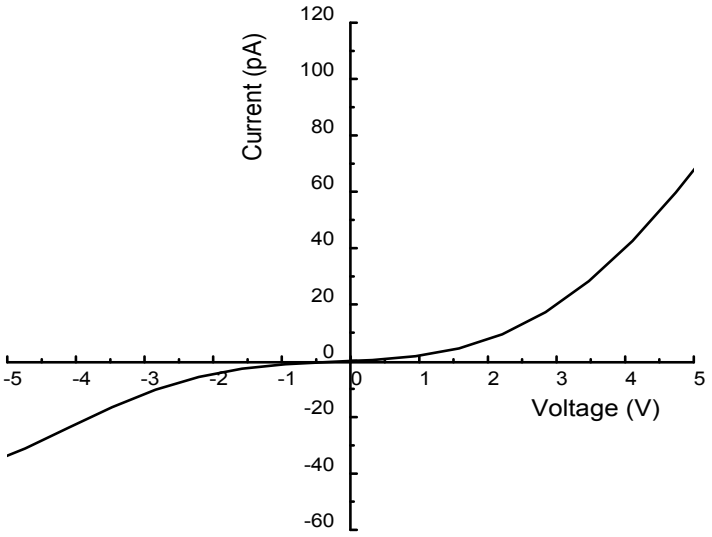

(a)

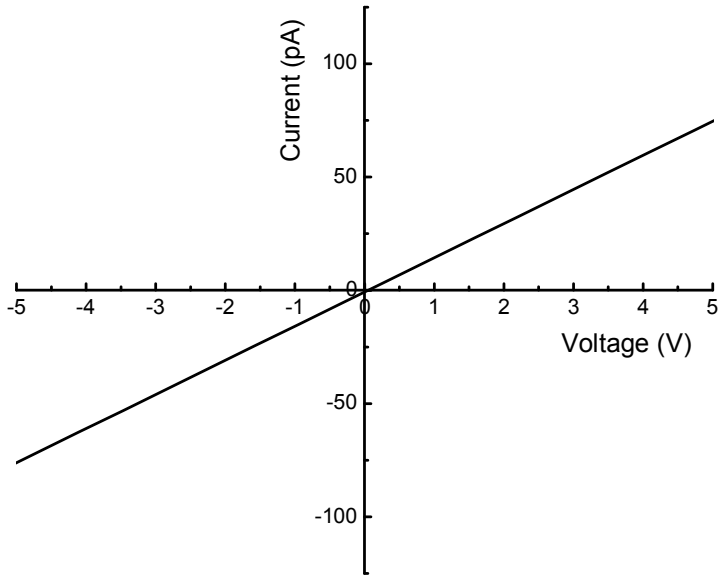

(b)

Figure 3.24: I-V characteristic of single ZnO platelet device (a) non linear behavior and (b) linear behavior.

3.4.3 Piezopotential Calculation for ZnO Nanoplatelets

Due to the high resistance of ZnO platelets, we expected that the piezopotential that the ZnO platelet could produce will be higher than ZnO nanowires. Gao [78] has pointed out that in ZnO nanowires the free electrons tend to accumulate at the positive potential side of the nanowire at thermal equilibrium. Therefore, the positive piezoelectric potential will be partially screened by the effect of free carriers, while the negative piezoelectric potential will not be influenced. Consequently, the overall piezopotential is reduced by the presence of free carriers. If the resistance of the semiconductor is high, on the contrary, the screening effect of free carriers will be reduced, resulting in higher piezopotential.

In addition, in 2006 Zhang et al. published a paper regarding the young's moduli of ZnO nanoplates [129]. They used density functional theory to calculate the Young's moduli of ZnO plates. Their results show that the Young's moduli substantially increases as size decreases. Therefore, the piezopotential will also be increased due to the increased elastic moduli.

Thus, in the following section, some preliminary calculation results for piezoelectric potential distribution in ZnO platelet are included. The software we used is COMSOL. COMSOL multiphysics simulation environment integrates a number of predefined physics interfaces for applications ranging from fluid flow and heat transfer to structural mechanics and electromagnetic analyses. This

environment enables us to define material properties, source terms and boundary conditions as arbitrary functions of the dependent variables.

We first set the material parameters for ZnO in a material library. In the structural mechanics module, the hexagonal shape of ZnO the platelet was then set up. The diameter of the ZnO platelet is 3.5 μm with 30 nm in thickness. The c-axis is perpendicular to the surface of the ZnO platelet. A bending force of 80 nN is applied parallel to c-axis at the middle of one edge of the ZnO platelet. The opposite side of the ZnO platelet is grounded. The result is shown in figure 3.25.

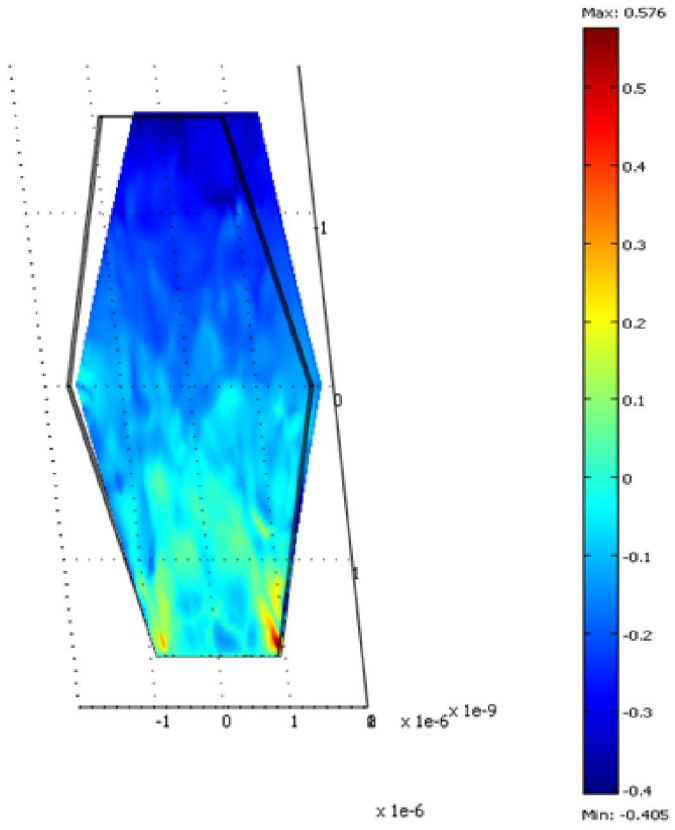

Figure 3.25: Piezoelectric potential distribution for ZnO platelet when a bending force of 80 nN is applied parallel to c-axis at the edge of ZnO platelet (thickness=30 nm).

The piezoelectric potential between two edges is about 0.405V, same as that of a ZnO nanowire. For the case of a ZnO nanowire, the piezoelectric potential distribution for a nanowire with diameter = 50 nm and length = 600 nm could be found in [130]. The root of the ZnO nanowire was also grounded. The piezoelectric potential is about 0.405V.

Since the Young's moduli of ZnO nanoplates depends on the thickness of ZnO platelet [129], the calculation was also done for a thinner ZnO platelet. For example, figure 3.26 shows the potential distribution for a ZnO platelet with thickness = 25 nm. The piezoelectric potential between two edges is about 0.483 V and it is indeed higher than that of platelet with thickness = 30 nm.

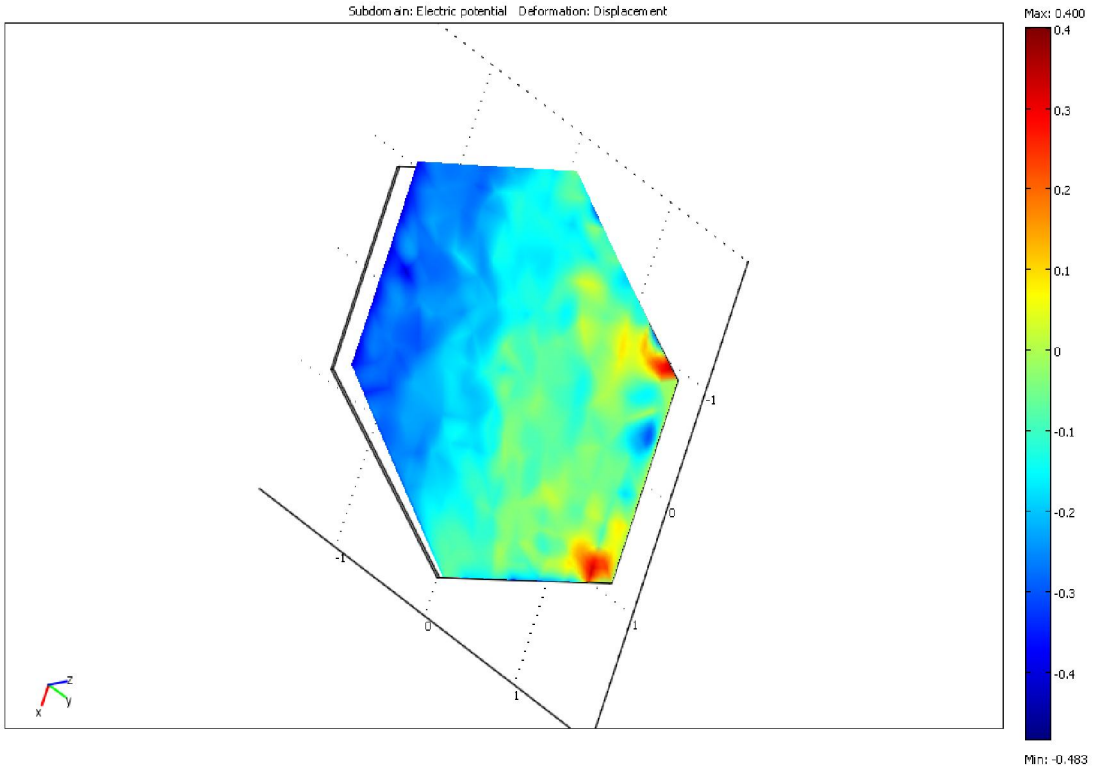

Figure 3.26: Piezoelectric potential distribution for thin ZnO platelet (thickness = 25 nm).

Unlike the ZnO nanowire, the piezoelectric potential distribution is across the surface of the plate. The potential is the same for front side and the back side. And the potential is set up between the two opposite edges of ZnO platelet. Thus, it is more convenient to make a nanogenerator with this kind of crystal and the expected output is also higher than that of ZnO nanowires. Details in experiment design and results are expected in future work.

Chapter 4
Conclusions and Future Work

4.1 Conclusions

In this thesis, approaches have been successful developed to synthesize ZnO nanocones and platelets. With the aid of UV illumination, ZnO nanocones could form by a low cost and high yield chemical approach on GaN film or gold film on sapphire and silicon substrates, respectively. Both TEM and XRD results show that as-grown ZnO nanocones are single crystals, although the side surface is not as flat as ZnO nanowires. The formation of ZnO nanocones could be understood by the absorption process of photons. The solution is not transparent to UV illumination and the substrate also strongly absorbs the light with energy larger than its band gap. Thus the solution is directly heated by the UV light and heated from above by the substrate. The local temperature of the solution near the substrate is higher than the temperature of the solution further from the substrate. Therefore, the UV light induced thermal gradient was set up that modified the heat distribution as well as the reagent transport. The chemical reaction system is kinetically limited. The a-axis growth speed near the substrate is faster than it is near the top of the nanostructure so the nanocone morphology is formed. In addition, the density of ZnO nanocones is higher than ZnO

nanowires grown without UV illumination since photons provide additional energy to overcome nucleation barriers.

By a chemical approach, ZnO platelets could be obtained on GaN film deposited by PLD, whose c-axis is parallel to the surface of the substrate. The diameters of ZnO platelets range from 2 μm to 25 μm and the thickness varies from 20 nm to 50 nm. Both of them depend on the quality and thickness of GaN film. TEM results illustrate that the obtained ZnO platelets are single crystalline grown along the <0 1 $\bar{1}$ 0> direction within the {0 0 0 1} planes. For ZnO crystal under hydrothermal conditions, the growth velocities are $V_{<0\,0\,0\,1>} > V_{<0\,1\,\bar{1}\,0>}$. However, relative growth rates of various facets were altered by the presence of [1 0 0] textured GaN film. We supposed that the suppression effect likely originates from the stress applied by the [1 0 0] textured GaN film on the ZnO nuclei. So ZnO plates grow along the six directions of <0 1 $\bar{1}$ 0> and leads to the formation of hexagonal platelets. Suppression of the growth along +c axis can also be achieved by citrate anions as structure-directing agents to adsorb selectively on ZnO basal planes. Electrical measurement shows that the resistance of ZnO platelets is about 20-40 GΩ and it is higher than ZnO nanowires. Piezoelectric potential calculation results indicate a good candidate for a piezoelectric device since the potential is higher than ZnO nanowires with the same external applied stress.

4.2 Future Work

As we pointed out in chapter 2, the morphology of nanowires is not the ideal shape of solar cells due to the matter of effective surface area as well as the strong reflection. Nanocone structures provides an alternative to further increase the efficiency of nanowire based solar cells. Thus, nanocone based solar cells should be fabricated and tested in future work.

As for ZnO platelets, work regarding to the formation of ZnO platelets should be set up in order to further analyze the mechanism of ZnO platelets growth. In addition, because of the high resistance and predicted piezoelectric potential, experimental piezoelectric measurement should be preformed and the design of ZnO platelets based nanogenerators undertaken.

References

[1] U. Ozgur, Y.I. Alivov, C. Liu, A. Teke, M.A. Reshchikov, S. Dogan, V. Avrutin, S.J. Cho and H. Morkoc “A comprehensive review of ZnO materials and devices”, J. Appl. Phys., 98 (2005), 041301.

[2] Z.L. Wang and J.H. Song “Piezoelectric nanogenerators based on zinc oxide nanowire arrays”, Science, 312 (2006), 242-246.

[3] X.D. Wang, J.H. Song, J. Liu and Z.L. Wang “Direct-Current nanogenerator driven by ultrasonic waves”, Science, 316 (2007), 102-105.

[4] S. Xu, Y.G. Wei, J. Liu, R.S. Yang and Z.L. Wang “Integrated multilayer nanogenerator fabricated using paired nanotip-to-nanowire brushes”, Nano Letters., 8 (2008), 4027-4032.

[5] R.S. Yang, Y. Qin, L.M. Dai and Z.L. Wang “Power generation with laterally packaged piezoelectric fine wires”, Nat. Nanotechnol., 4 (2009), 34.

[6] X.D. Wang, J. Liu, J.H. Song and Z.L. Wang “Integrated nanogenerators in biofluid”, Nano letters., 7 (2007), 2475-2479.

[7] Y. Qin, X.D. Wang and Z.L. Wang “Microfibre-nanowire hybrid structure for energy scavenging”, Nature, 451 (2008), 809.

[8] R.S. Yang, Y. Qin, C. Li, G. Zhu, and Z.L. Wang “Converting biomechanical energy into electricity by a muscle-movement-driven nanogenerator”, Nano Lett., 9 (2009), 1201-1205.

[9] S. Xu, Y. Qin, C. Xu, Y. Wei, R.S. Yang, and Z.L. Wang “Self-powered nanowire devices”, Nat. Nanotechnol., 5 (2010), 366-373.

[10] E. Klimiec, W. Zaraska, K. Zaraska, K.P. Gasiorski, T. Sadowski and M. Pajda “Piezoelectric polymer films as power converters for human powered electronics”, Micorelectron. Reliab., 48 (2008), 891-901.

[11] Z. Li, G. Zhu, R.S. Yang, A.C. Wang and Z.L. Wang “Muscle-driven in vivo nanogenerator”, Adv. Mater., 22 (2010), 1-4.

[12] B.J. Hansen, Y. Liu, R.S. Yang and Z.L. Wang “Hybrid nanogenerator for concurrently harvesting biomechanical and biochemical energy”, ACS nano, online.

[13] J. Liu, P. Fei, J. Zhou, R. Tummala and Z.L. Wang “Toward high output-power nanogenerator”, Appl. Phys. Lett., 92 (2008), 173105.

[14] M.P. Lu, J.H. Song, M.Y. Lu, M.T. Chen, Y.F. Gao, L.J. Chen and Z.L. Wang “Piezoelectric nanogenerator using p-type ZnO nanowire arrays”, Nano Letters., 9 (2009), 1223-1227.

[15] C.T. Huang, J.H. Song, W.F. Lee, Y. Ding, Z.Y. Gao, Y. Hao, L.J. Chen and Z.L. Wang “GaN nanowire arrays for high-output nanogenerators”, J. AM. CHEM. SOC., online.

[16] Y.F. Lin, J.H. Song, Y. Ding, S.Y. Liu and Z.L. Wang “Piezoelectric nanogenerator using CdS nanowires”, Appl. Phys. Lett., 92 (2008), 022105.

[17] Y.F. Lin, J.H. Song, Y. Ding, S.Y. Lu and Z.L. Wang “Alternating the output of a CdS nanowire nanogenerator by a white-light-stimulated optoelectronic effect”, Adv. Mater., 20 (2008), 3127.

[18] M.Y. Lu, J.H. Song, M.P. Lu, C.Y. Lee, L.J. Chen and Z.L. Wang “ZnO/ZnS heterojunction and ZnS nanowire arrays for electricity generation”, ACS Nano, 3 (2009), 357-362.

[19] F.H. Nicoll “Ultraviolet ZnO laser pumped by an electron beam”, Appl. Phys. Lett., 9 (1966), 13-15.

[20] D.M. Bagnall, Y.F. Chen, Z. Zhu, T. Yao, S. Koyama, M.Y. Shen and T. Goto “Optically pumped lasing of ZnO at room temperature”, Appl. Phys. Lett., 70 (1997), 2230-2232.

[21] M.A. Zimmler, J. Bao, F. Capasso, S. Muller and C. Ronning “Laser action in nanowires: observation of the transition from amplified spontaneous emission to laser oscillation”, Appl. Phys. Lett., 93 (2008), 051101.

[22] A. Tsukazaki, A. Ohtomo, T. Onuma, M. Ohtani, T. Makino, M. Sumiya, K. Ohtani, S.F. Chichibu, S. Fuke, Y. Segawa, H. Ohno, H. Koinuma and M. Kawasaki “Repeated temperature modulation epitaxy for p-type doping and light-emitting diode based on ZnO”, Nat. Mater. 4 (2005), 42-46.

[23] Y. Ryu, T.S. Lee, J.A. Lubguban, H.W. White, B.J. Kim, Y.S. Park “Next generation of oxide photonic devices: ZnO-based ultraviolet light emitting diodes”, Appl. Phys. Lett., 88 (2006), 241108.

[24] J. Bao, M.A. Zimmler and F. Capasso “Broadband ZnO single nanowire light emitting diode”, Nano Lett., 6 (2006), 1719-1722.

[25] X.M. Zhang, M.Y. Lu, Y. Zhang, L.J. Chen and Z.L. Wang “Fabrication of a high-brightness blue-light-emitting diode using a ZnO nanowire array grown on p-GaN thin film”, Adv. Mater., 21 (2009), 2767-2770.

[26] J.B. Baxter and E.S. Aydil “Nanowire-based dye-sensitized solar cells”, Appl. Phys. Lett., 86 (2005), 053114.

[27] M. Law, L. Greene, J.C. Johnson, R. Saykally and P. Yang “Nanowire dye-sensitized solar cells”, Nat. Mater., 4 (2005), 455-459.

[28] B. Weintraub, Y. Wei and Z.L. Wang “Optical fiber/nanowire hybrid structures for efficient three-dimensional dye-sensitized solar cells”, Angew. Chem., Int. Ed. 48 (2009), 1-6.

[29] J.D. Albrecht, P.P. Ruden, S. Limpijumnong, W.R.L. Lambrecht and K.F. Brennan “High field electron transport properties of bulk ZnO”, J. Appl. Phys., 86 (1999), 6864.

[30] D.C. Look, J.W. Hemsky and J.R. Sizelove “Residual native shallow donor in ZnO”, Phys. Rev. Lett., 82 (1999), 2552.

[31] D.C. Look, D.C. Reynolds, J.R. Sizelove, R.L. Jones, C.W. Litton, G. Cantwell and W.C. Harsch “Electrical properties of bulk ZnO”, Solid State Commun. 105 (1998) 399-401.

[32] E.M. Kaidashev, M. Lorenz, H.V. Wenckstern, A. Rahm, H.C. Semmelhack, K.H. Han, G. Benndorf, C. Bundesmann, H. Hochmuth and M. Grundmann “High electron mobility of epitaxial ZnO thin films on c-plane sapphire grown by multistep pulsed-laser deposition”, Appl. Phys. Lett., 82 (2003), 3901.

[33] H. Kato, M. Sano, K. Miyamoto and T. Yao “Effect of O/Zn flux ratio on crystalline quality of ZnO films grown by plasma-assisted molecular beam epitaxy” Jpn. J. Appl. Phys., 42 (2003), 2241-2244.

[34] J. Nause and B. Nemeth “Pressurized melt growth of ZnO boules” Semicond. Sci. Technol., 20 (2005), S45-S48.

[35] K. Maeda, M. Sato, I. Niikura and T. Fukuda “Growth of 2 inch ZnO bulk single crystal by the hydrothermal method”, Semicond. Sci. Technol., 20 (2005), S49-S54.

[36] A. Ohtomo and A. Tsukazaki “Pulsed laser deposition of thin films and superlattices based on ZnO”, Semicond. Sci. Technol., 20 (2005), S1-S12.

[37] J.Y. Park, H. Oh, J.J. Kim and S.S. Kim “The temperature-dependent electrical transport mechanism of single ZnO nanorod”, Nanotechnology, 17 (2006), 1255-1259.

[38] Y.W. Heo, L.C. Tien, D.P. Norton, B.S. Kang, F. Ren, B.P. Gila and S.J. Pearton “Electrical transport properties of single ZnO nanorods”, Appl. Phys. Lett., 85 (2004), 2002.

[39] Y.J. Ma, Z. Zhang, F. Zhou, L. Lu, A. Jin and C. Gu “Hopping conduction in single ZnO nanowires”, Nanotechnology, 16 (2005), 746.

[40] Z.Y. Zhang, C.H. Jin, X.L. Liang, Q. Chen and L.M. Peng “Current-voltage characteristics and parameter retrieval of semiconducting nanowires”, Appl. Phys. Lett., 88 (2006), 073102.

[41] Z.M. Liao, K.J. Liu, J.M. Zhang, J. Xu and D.P. Yu “Effect of surface states on electron transport in individual ZnO nanowires”, Phys. Lett. A, 367 (2007), 207.

[42] Y.F. Lin, W.B. Jian, C.P. Wang, Y.W. Suen, Z.Y. Wu, F.R. Chen, J.J. Kai and J.J. Lin “Contact to ZnO and intrinsic resistances of individual ZnO nanowires with a circular cross section”, Appl. Phys. Lett., 90 (2007), 223117.

[43] A. Umar, B.K. Kim, J.J. Kim and Y.B. Hahn “Optical and electrical properties of ZnO nanowires grown on aluminum foil by non-catalytic thermal evaporation ”,Nanotechnology, 16 (2007), 175606.

[44] Y.W. Heo, L.C. Tien, D.P. Norton, S.J. Pearton, B.S. Kang, F. Ren and J.R. Laroche “Pt/ZnO nanowire Schottky diodes”, Appl. Phys. Lett., 85 (2004), 3107.

[45] P.C. Chang, Z. Fan, C.J. Chien, D. Stichtenoth, C. Ronning and J.G. Lu “High performance ZnO nanowire field effect transistors”, Appl. Phys. Lett., 89 (2006), 133113.

[46] P.C. Chang, C.J. Chien, D. Stichtenoth, C. Ronning and J.G. Lu “Finite size effect in ZnO nanowires”, Appl. Phys. Lett., 90 (2007), 113101.

[47] X. Lin, X.B. He, T.Z. Yang, W. Guo, D.X. Shi, H.J. Gao, D.D. Ma, S.T. Lee, F. Liu and X.C. Xie “Intrinsic current-voltage properties of nanowires with four-probe scanning tunneling microscopy: A conductance transition of ZnO nanowire”, Appl. Phys. Lett., 89 (2006), 043103.

[48] J. Goldberger, D.J. Sirbuly, M. Law and P. Yang “ZnO nanowire transistors”, J. Phys. Chem. B, 109 (2005), 9.

[49] W. I.I. Park, J.S. Kim, G.C. Yi, M.H. Bae and H.J. Lee “Fabrication and electrical characteristics of high-performance ZnO nanorod field-effect transistors”, Appl. Phys. Lett., 85 (2004), 5052.

[50] Q.H. Li, Q. Wan, Y.X. Liang and T.H. Wang “Electronic transport through individual ZnI nanowires”, Appl. Phys. Lett., 84 (2004), 4556.

[51] Q.H. Li, Y.X. Liang, Q. Wang and T.H. Wang “Oxygen sensing characteristics of individual ZnO nanowire transistors”, Appl. Phys. Lett., 85 (2004), 6389.

[52] Z. Fan, D. Wang, P.C. Chang, W.Y. Tseng and J.G. Lu “ZnO nanowire field-effect transistor and oxygen sensing property”,Appl. Phys. Lett., 85 (2004), 5923.

[53] C.S. Lao, J. Liu, P. Gao, L. Zhang, D. Davidovic, R. Tummala R and Z.L. Wang “ZnO nanobelt/nanowire Schottky diodes formed by dielectrophoresis alignment across Au electrodes”, Nano Lett., 6 (2006), 263.

[54] L.J. Brillson, H.L. Mosbacker, M.J. Hetzer, Y. Strzhemechny, G.H. Jessen, D.C. Look, G. Cantwell, J. Zhang and J.J. Song “Dominant effect of near-interface native point defects on ZnO Schottky barriers”, Appl. Phys. Lett., 90 (2007), 102116.

[55] Y. Ding and Z.L. Wang “Structure analysis of nanowires and nanobelts by transmission electron microscopy”, J. Phys. Chem. B, 108 (2004), 12280.

[56] S.E. Harrison “Conductivity and Hall effect of ZnO at low temperatures”, Phys. Rev., 93 (1954), 52.

[57] D.G. Look, J.W. Hemsky and J.R. Sizelove “Residual native shallow donor in ZnO”, Phys. Rev. Lett., 82 (1999), 2552.

[58] A. Janotti, C. Van de Walle “Native point defects in ZnO”, Phys. Rev. B, 76 (2007), 165202.

[59] B. Postels, H.H. Wehmann, A. Bakin, M. Kreye, D. Fuhrmann, J. Blaesing, A. Hangleiter, A. Krost and A. Waag “Controlled low-temperature fabriction of ZnO nanopillars with a wet-chemical approach”, Nanotechnology, 18 (2007), 195602.

[60] J. Appenzeller, M. Radosavljevic, J. Knoch and P. Avouris “Tunneling versus thermionic emission in one-dimensonal semiconductors”, Phys. Rev. Lett., 92 (2004), 048301.

[61] F.A. Padovani, R. Stratton “Field and thermionic-field emission in Schottky barriers”, 9 (1966), 695.

[62] H. Kind, H. Yan, B. Messer, M. Law and P. Yang “Nanowire ultraviolet photodetectors and optical switches”, Adv. Mater., 14 (2002), 158.

[63] E. Schlenker, A. Bakin, T. Weimann, P. Hinze, D.H. Weber, A. Golzhauser, H.H. Wehmann and A. Waag “On the difficulties in characterizing ZnO nanowires”, Nanotechnology, 19 (2008), 465707.

[64] A.A. Tomchenko, G.P. Harmer, B.T. Marquis and J.W. Allen “Semiconducting metal oxide sensor array for the selective detection of combustion gases”, Sens. Actuators B, 93 (2003), 126.

[65] T.Y. Wei, P.H. Yeh, S.Y. Lu and Z.L. Wang “Gigantic enhancement in sensitivity using Schottky contacted nanowire nanosensor”, J. Am. Chem. Soc., 131 (2009), 17690-17695.

[66] P. Yang, H. Yan, S. Mao, R. Russo, J. Johnson, R. Saykally, N. Morris, J. Pham, R. He and H.J. Choi “Controlled growth of ZnO nanowires and their optical properties”, Adv. Funct. Mater., 12 (2002), 323-331.

[67] K. Vanheusden, W.L. Warren, C.H. Seager, D.R. Tallant, J.A. Voigt, B.E. Gnage “Mechanisms behind green photoluminescence in ZnO phosphor powders”, J. Appl. Phys., 79 (1996), 7983.

[68] H. Kind, H. Yan, B. Messer, M. Law and P. Yang “Nanowire ultraviolet photodetectors and optical switches”, Adv. Mater., 14 (2002), 158-160.

[69] K. Keem, H. Kim, G.T. Kim, J.S. Lee, B. Min, K. Cho, M.Y. Sung, and S. Kim “Photocurrent in ZnO nanowires grown from Au electrodes”, Appl. Phys. Lett., 84 (2004), 4376.

[70] Y.Y. Lin, C.W. Chen, W.C. Yen, W.F. Su, C.H. Ku and J.J. Wu “Near-ultraviolet photodetector based on hybrid polymer/zinc oxide nanorods by low-temperature solution processes”, Appl. Phys. Lett., 92 (2008), 233301.

[71] C.S. Lao, M.C. Park, Q. Kuang, Y. Deng, A.K. Sood, D.L. Polla and Z.L. Wang “Giant enhancement in UV response of ZnO nanobelts by polymer surface functionalization”, J. Am. Chem. Soc., 129 (2007), 12096.

[72] S.E. Ahn, H.J. Ji, K. Kim, G.T. Kim, C.H. Bae, S.M. Park, Y.K. Kim and J.S. Ha “Origin of the slow photoresponse in an individual sol-gel synthesized ZnO nanowire”, Appl. Phys. Lett., 90 (2007), 153106.

[73] Y.B. Li, F.D. Valle, M. Simonnet, I. Yamada and J.J. Delaunay “Competitive surface effects of oxygen and water on UV photoresponse of ZnO nanowires”, Appl. Phys. Lett., 94 (2009), 023110.

[74] R.S. Aga, D. Jowhar, A. Ueda, Z. Pan, W.E. Collins, R. Mu, K.D. Singer and J. Shen “Enhanced photoresponse in ZnO nanowires decorated with CdTe quantum dot”, Appl. Phys. Lett., 91 (2007), 232108.

[75] J. Zhou, Y. Gu, Y. Hu, W. Mai, P.H. Yeh, G. Bao, A.K. Sood, D.L. Polla and Z.L Wang “Gigantic enhancement in response and reset time of ZnO UV nanosensor by utilizing Schottky contact and surface functionalization”, Appl. Phys. Lett., 94 (2009), 191103.

[76] Y.F. Hu, Y.L. Chang, P. Fei, R.L. Snyder and Z.L. Wang “Designing the electric transport characteristics of ZnO Micro/Nanowire devices by coupling piezoelectric and photoexcitation effects”, ACS Nano, 4 (2010), 1234-1240.

[77] Z.L. Wang “Piezotronic and piezophototronic effects”, J. Phys. Chem. Lett., 1 (2010), 1388-1393.

[78] Z.Y. Gao, J. Zhou, Y.D. Gu, P. Fei, Y. Hao, G. Bao and Z.L. Wang “Effects of piezoelectric potential on the transport characteristics of metal-ZnO nanowire-metal field effect transistor”, J. Appl. Phys. Lett., 105 (2009), 113707.

[79] Y.F. Hu, Y. Zhang, Y.L. Chang, R.L. Snyder and Z.L. Wang “Optimizing the power output of a ZnO photocell by piezopotential”, ACS Nano, online.

[80] Z.L. Wang “ZnO nanowire and nanobelt platform for nanotechnology”, Mater. Sci. Eng., R 64 (2009), 33.

[81] X.F. Duan, Y. Huang, R. Agarwal, and C.M. Lieber “Single-nanowire electrically driven lasers”, Nature, 421 (2003), 241.

[82] Y. Dai, Y. Zhang, and Z.L. Wang “The octa-twin tetraleg ZnO nanostructures” Solid State Commun., 126 (2003), 629.

[83] X.Y. Kong and Z.L. Wang “Spontaneous Polarization-Induced Nanohelixes, Nanosprings, and Nanorings of Piezoelectric Nanobelts”, Nano Lett., 3 (2003), 1625.

[84] X.Y. Kong, Y. Ding, R. Yang, and Z.L. Wang “Single-Crystal Nanorings Formed by Epitaxial Self-Coiling of Polar Nanobelts”, Science, 303 (2004),1348.

[85] P.X. Gao and Z.L. Wang “Nanoarchitectures of semiconducting and piezoelectric zinc oxide”, J. Appl. Phys., 97 (2005), 044304.

[86] P.X. Gao, Y. Ding, W.J. Mai, W.L. Hughes, C.S. Lao, and Z.L. Wang “Conversion of Zinc Oxide Nanobelts into Superlattice-Structured Nanohelices” Science, 309 (2005), 1700.

[87] W.L. Hughes, and Z.L. Wang “Formation of Piezoelectric Single-Crystal Nanorings and Nanobows” J. Am. Chem. Soc., 126 (2004) 6703.

[88] C.S. Lao, P.X. Gao, R.S. Yang, Y. Zhang, Y. Dai, and Z.L. Wang “Formation of double-side teethed nanocombs of ZnO and self-catalysis of Zn-terminated polar surface” Chem. Phys. Lett., 417 (2005),358.

[89] M.H. Huang, S. Mao, H. Feick, H.Q. Yan, Y.Y. Wu, H. Kind, E. Weber, R. Russo and P.D. Yang “Catalytic growth of Zinc oxide nanowires by vapor transprot”, Adv. Mater., 13 (2001), 113.

[90] X.F. Duan and C.M. Lieber “General synthesis of compound semiconductor nanowires”, Adv. Mater., 12 (2000), 298.

[91] R. Konenkamp, K. Boedecker, M.C. Lux-Steiner, M. Poschenrieder, F. Zenia, C.L. Clement and S. Wagner “Thin film semiconductor deposition on free-standing ZnO columns”, Appl. Phys. Lett., 77 (2000), 2575.

[92] R. Liu, A.A. Vertegel, E.W. Bohannan, T.A. Sorenson, J.A. Switzer “Epitaxial electrodeposition of Zinc oxide nanopillars on single crystal gold”, Chem. Mater., 13 (2001), 508.

[93] J.J. Wu and S.C. Liu “Low-temperature growth of well-aligned ZnO nanorods by chemical vapor deposition”, Adv. Mater., 14 (2002), 215.

[94] S. Xu, C.S. Lao, B. Weintraub and Z.L. Wang “Density-controlled growth of aligned ZnO nanowire arrays by seedless chemical approach on smooth surfaces”, J. Mater. Res., 23 (2008), 2072.

[95] S. Xu, Y.G. Wei, M. Kirkham, J. Liu, W.J. Mai, D. Davidovic, R.L. Snyder and Z.L. Wang “Patterned growth of vertically aligned ZnO nanowire arrays on inorganic substrates at low temperature without catalyst”, J. Am. Chem. Soc., 130 (2008), 14958.

[96] J. J. Urban, D. V. Talapin, E. V. Shevchenko, C. R. Kagan, and C. B. Murray “Synergism in binary nanocrystal superlattices leads to enhanced p-type conductivity in self-assembled PbTe/Ag_2Te thin films”, Nat. Mater., 6 (2007), 115.

[97] Y. Li, F. Qian, J. Xiang, and C. M. Lieber ” Nanowire electronic and optoelectronic devices ”, Mater. Today 9 (2006), 18.

[98] L. Zhang, R. Tu, and H. Dia “Parallel Core−Shell Metal-Dielectric-Semiconductor Germanium Nanowires for High-Current Surround-Gate Field-Effect Transistors”, Nano Lett. 6, (2006) 2785.

[99] M. Law, L. E. Greene, A. Radenovic, T. Kuykendall, J. Liphardt, and P.Yang “ZnO−Al_2O_3 and ZnO−TiO_2 Core−Shell Nanowire Dye-Sensitized Solar Cells” J. Phys. Chem. B, 110 (2006), 22652.

[100] M. Law, L.E. Greene, J.C. Johnson, R. Saykally and P. Yang “Nanowire dye-sensitized solar cells”, Nat. Mater., 4 (2005), 455.

[101] J. Zhu, Z.F. Yu, G.F. Burkhard, C.M. Hsu, S.T. Connor, Y.Q. Xu, Q. Wang, M. McGehee, S.H. Fan and Yi Cui “Optical absorption enhancement in amorphous silicon nanowire and nanocone arrays”, Nano. Lett., 9 (2009), 279-282.

[102] S.H. Lee, X.G. Zhang, B. Smith, S.S. Seo, Z.W. Bell and J. Xu “ZnO-ZnTe nanocone heterojunctions”, Appl. Phys. Lett., 96 (2010), 193116.

[103] J. Bae, JI. Hong, W.H. Han, Y.J. Choi and R.L. Snyder “Superior Field Emission Properties of ZnO Nanocones Synthesized by Pulsed Laser Deposition”, Chem. Phys. Lett., 475 (2009), 260.

[104] J. Bae, E.L. Shim, T.Y. Park, C.J. Kang and Y.J. Choi “Formation of ZnO nanocones using wet chemical etching of ZnO nanorods in an aqueous solution of HCL”, J. Nanosci. Nanotechnol., 9 (2009), 7398.

[105] C. Fauteux, R. Longtin, J. Pegna and D. Therriault “Fast synthesis of ZnO nanostructures by laser-induced decomposition of Zinc acetylacetonate”, Inorg. Chem., 46 (2007), 11036-11047.

[106] D.A. Porter “Phase Transformations in metals and alloys”, second edition.

[107] H.T. Ng, J. Li, M.K. Smith, P. Nguyen, A. Cassell, J. Han and M. Meyyappan “Growth of Epitaxial Nanowires at the Junctions of Nanowalls”, Science, 300 (2003), 1249.

[108] N. Wang, H. Lin, J.B. Li, L.Z. Zhang, X. Li, J. Wu and C.F. Li “Strong Orange Luminescence from a Novel Hexagonal ZnO Nanosheet Film Grown on Aluminum Substrate by a Simple Wet-Chemical Approach”, J. Am. Ceram. Soc., 90 (2007), 635.

[109] C.H. Ye, Y. Bando, G.Z. Shen and D. Golberg “Thickness-dependent photocatalytic performance of ZnO nanoplatelets”, J. Phys. Chem. B, 110 (2006), 15146.

[110] M.S. Akhtar, J.H. Hyung, O.B. Yang, N.K. Cho, H.I. Hwang and S.K. Lee “Thermally grown ZnO nanosheets for high efficiency dye-sensitized solar cells”, J. Nanosci. Nanotechnol., 10 (2010), 3654-3685.

[111] E. Hosono, S.B. Fujihara, I. Honma and H. Zhou “The fabrication of an upright-standing Zinc oxide nanosheet for use in dye-sensitized solar cells”, Adv. Mater., 17 (2005), 2091.

[112] S.J. Chen, Y.C. Liu, C.L. Shao, R. Mu, Y.M. Lu, J.Y. zhang, D.Z. Shen and X.W. Fan “Structural and optical properties of uniform ZnO nanosheets”, Adv. Mater., 17 (2005),586.

[113] C.X. Xu, X.W. Sun, Z.L Dong and M.B. Yu “Zinc oxide nanodisk”, Appl. Phys. Lett., 85 (2004), 3878.

[114] A. Umar and Y.B. Hahn “ZnO nanosheet networks and hexagonal nanodiscs grown on silicon substrate: growth mechanism and structural and optical properties ”, Nanotechnology, 17 (2006), 2174.

[115] J.Q. Hu, Y. Bando, J.H. Zhan, Y.B. Li and T. Sekiguchi “Two-dimensional micrometer-sized single-crystalline ZnO thin nanosheets”, Appl. Phys. Lett., 83 (2003),4414.

[116] J.H. Park, Y.J. Choi and J.G. Park “Synthesis of ZnO nanowires and nanosheets by an O2-assisted carbothermal reduction process”, J. Cryst. Growth, 280 (2005), 161.

[117] J.H. Park, H.J. Choi, Y.J. Choi, S.H. Sohn and J.G. Park “Ultrawide Zno nanosheets”, J. Mater. Chem., 14 (2004), 35.

[118] B.Q. Cao, W.P. Cai, Y. Li, F.Q. Sun and L.D. Zhang “Ultraviolet-light-emitting ZnO nanosheets prepared by a chemical bath deposition method”, Nanotechnology, 16 (2005), 1734.

[119] F. Xu, Z.Y. Yuan, G.H. Du, M. Halasa and B.L. Su “High-yield synthesis of single-crystalline ZnO hexagonal nanoplates and accounts of their optical and photocatalytic properties ”, Appl. Phys. A., 86 (2007), 181.

[120] X.Y. Chen, X.F. Zhang, Z.J. Zhang, J.W. Liu and Y.T. Qian “A precursor-growth-pyrolysis approach to two-dimensional ZnO micro-platelets with hexagonal morphologies”, J. Cryst. Growth, 280 (2005), 244.

[121] J.I. Hong, Y.L. Chang, Y. Ding, Z.L. Wang and R. L. Snyder “Growth of GaN films with controlled out-of-plane texture on Si wafers”, Physica Status Solidi-Rapid Research Letters submitted.

[122] J.I. Hong, J. Bae, Z.L. Wang and R.L. Snyder “Room-temperature, texture-controlled growth of ZnO thin films and their application for growing aligned ZnO nanowire arrays”, Nanotechnology, 20 (2009), 085609.

[123] W.J. Li, E.W. Shi, W.Z. Zhong and Z.W. Yin “Growth mechanism and growth habit of oxide crystals”, J. Cryst. Growth, 203 (1999), 186.

[124] Z. Tian, J.A. Voigt, J. Liu, B. Mchenzie, M.J. Mcdermott, M.A. Rodriguez, H. Konishi and H. Xu “Complex and oriented ZnO nanostrucures”, Nat. Mater., 12 (2003), 821.

[125] E.H. Rhoderick and R.H. Williams “Metal-Semiconductor contacts”, oxford university press, USA.

[126] David R. Lide, “CRC handbook on Chemistry and Physics” version 2008, p. 12-114.

[127] S.A. Campbell “Fabrication engineering at the micro and nanoscale” (3rd edition), Oxford University Press, 2008.

[128] U.N. Maiti, K.K. Chattopadhyay, S. Karan and B. Mallik “Synthesis of a zinc oxide nanosheet-nanowire network complex by a low-temperature chemical route: efficient UV detection and field emission property”, Scripta Materialia 62 (2010), 305.

[129] L.X. Zhang and H.C. Huang “Young’s moduli of ZnO nanoplates: Ab initio determinations”, Appl. Phys. Lett., 89 (2006), 183111.

[130] Y.F. Gao and Z.L. Wang “Electrostatic potential in a bent piezoelectric nanowire. The fundamental theory of nanogenerator and nanopiezotronics”, Nano. Lett., 7 (2007), 2499.